Iranian Journal of Geophysics, Vol 18 No 6, 2025, Page 47 – 78 (Research Article)
DOI: 10.30499/ijg.2024.431927.1559

Evaluation of the groundwater potential of Ogbomoso, Southwestern Nigeria, using an adaptive neuro-fuzzy inference system optimized by three metaheuristic algorithms

Timothy Pelumi Fajemilo [1] and Kesyton Oyamenda Ozegin [2*]

[1] *M.Sc. Graduate, Department of Applied Geophysics, Federal University of Technology, Akure, Nigeria*
[2] *Ph.D., Department of Physics, Ambrose Alli University Ekpoma, Edo State, Nigeria*

(Received: 23 December 2023, Accepted: 24 April 2024)

Abstract

Groundwater is a significant driver of water supply considering its constant accessibility, intrinsic quality, and ease of immediate diversion to disadvantaged areas. The bulk of the Ogbomoso population relies on surface water because of normative groundwater investigation, which is a laborious and resource-intensive process. Over the last decade, the use of an adaptive neuro-fuzzy inference system (ANFIS) has garnered enthusiastic acceptance in a variety of research domains. This study aimed to evaluate groundwater potential in Ogbomoso, Nigeria, using ANFIS in a geographic information system coupled with three metaheuristic optimizing algorithms: the genetic algorithm (GA), particle swarm optimization (PSO), and the firefly algorithm (FA). To facilitate groundwater potential mapping (GPM) in the research area, a database of 165 wells with 8 predictive parameters was created. Thirty percent (49) of the 165 well locations were designated for the validation set, while the remaining seventy percent (116) were designated for the training set. The slope, lineament density, lithology, overburden thickness, bedrock relief, coefficient of anisotropy, hydraulic conductivity, and transmissivity were the eight groundwater variable parameters generated for modeling. The findings showed that each of the models had good prediction capability; nonetheless, the ANFIS-GA has the strongest predicting effectiveness with a correlation level of r = 0.8 (80%), followed by both the ANFIS-PSO and the ANFIS-FA with r = 0.77 (77%). The groundwater potential index developed for the study region was zoned into low (0.77–1.63) (30%), moderate (1.63–1.74) (25%), and high (1.74–2.50) (45%) using the ANFIS improved by the GA method. The linear correlation method was used to validate the model using 110 water columns from wells in the study area. The findings of this study demonstrate that ANFIS models paired with metaheuristic algorithmic optimization can be an invaluable tool for making decisions for groundwater utilization and monitoring.

Keywords: Machine learning, linear and non-linear models, ANFIS, genetic algorithm, performance evaluation, groundwater potential

[*]Corresponding author: ozeginkess@yahoo.com

1 Introduction

Groundwater has always been important to human existence. It is an invaluable asset that is essential to the survival of contemporary civilizations while also contributing to the preservation of land and aquatic environments. However, due to the geometric expansion of population, growing cities, and dearth of water, groundwater sources have received greater prominence. Since groundwater is a limited resource, exploring, understanding, and evaluating the groundwater potential of an area is necessary for sustainable use, especially in a basement complex terrain (Khabat et al., 2018; Das and Pardeshi, 2018; Bawallah et al., 2019; Ilugbo et al., 2023a). This informs the use of a model that can be used to accurately predict the groundwater in an area for sustainability. Ogbomoso in Nigeria with a population of approximately 245,000 (NPC, 2006) is a town with rapid population growth. Despite the rapid population growth and relative industrialization, Ogbomoso is destitute of pipe-borne water supply, which has resulted in a shortage of water demand for industrial and domestic needs for the inhabitants of the community. Also, the report of incessant borehole failures in the community cannot be overemphasized. The identification of potential watershed zoning constitutes one of the most effective techniques for regulating as well as preserving groundwater (see Tesfaye, 2014; Kumar et al., 2016; Hussein et al., 2017; Maniar et al., 2017; Maity et al., 2022; Ozegin et al., 2023; Ozegin and Ilugbo, 2024).

Numerous techniques exist for the potential zoning and utilization of groundwater. According to Todd and Mays (1980), Singh and Prakash (2002), Ozegin et al. (2007), Bawallah et al. (2019), Ilugbo et al. (2023a), and Idiahi et al. (2023), the most often employed conventional practices are drilling and geological, geophysical, and hydrogeological methods. However, particularly considering vast areas, they are labor-intensive and costly solutions. Due to their capacity to handle massive amounts of spatial data, GIS and remote sensing are now recognized as invaluable methods for evaluating groundwater potential (e.g., Deepesh et al., 2010; Fashae et al., 2014; Gopinathan et al., 2020).

More recently, several statistical approaches have been proposed, including the use of the frequency ratio (Ozdemir, 2011; Elmahdy and Mohamed, 2014; Das and Pardeshi, 2018), multifaceted decision evaluation (Sahoo et al., 2015; Jhan et al., 2012; Julla et al., 2022; Ozegin et al., 2023; Ozegin and Ilugbo, 2024), the logistical regression model (Zandi et al., 2016), evidence-based belief performance (Tahmassebipoor et al., 2016; Chen et al., 2018), the weight of evidence-geo-statistical method (Shenyong and Ruiqiu, 2001; Khosravi et al., 2016; Xu et al., 2012), and Shannon's randomness (Elvis et al., 2022), have been examined for ground water modeling. The multifaceted decision evaluation procedure is an indicator that is skewed because of the views of experts, whereas two-variate and multidimensional statistics have limitations in quantifying the link between the presence of groundwater and contextual variables (Tehrany et al., 2013; Umar et al., 2014). The capability of machine learning (ML) to effectively manage heterogeneous structured data from multiple sources at different scales has led to its consideration and efficiency. Additionally, there are no statistical presumptions needed for machine learning. A popular ML technique for hydrological modeling utilizes the artificial neural network (ANN) model (Karamouz et al., 2007; Corsini et al., 2009; Lee et al., 2012; Sokeng et al., 2016; Tsakiri et al., 2018; Lee et al., 2018) because it is

computationally efficient. However, a variety of hybrid models have been suggested since the ANN model contains multiple drawbacks, including low prediction accuracy and modeling uncertainty (Bui et al., 2016).

An Adaptive Neuro-Fuzzy Inference System (ANFIS) has been emerged as one of the most effective hybridized mechanisms for superior accuracy (e.g., Dehnavi et al., 2015; Rezaei et al., 2017; Chen et al., 2017; Hong et al., 2018; Milan et al., 2018; Khosravi et al., 2018; Termeh et al., 2019; Jaafari et al., 2019; Chen et al., 2019; Azad et al., 2019; Roy et al., 2020). It has demonstrated success in modeling a variety of procedures employed in hydrodynamics and engineering with regard to water resources by having the capacity and potential to combine the expressive strength of a fuzzy system with the numerical power of a neural network. The studying, creating, costing, and categorizing skills of ANFIS are strong. It can develop a rule base automatically by extracting fuzzy rules from quantitative information or domain expertise (Chang and Chang, 2006). ANFIS has been used by some scholars for projecting groundwater over the past few years (Affandi and Watanabe, 2007; Bisht et al., 2009; Amutha and Porchelvan, 2011; Mayilvaganan and Naidu 2012; Emamgholizadeh et al., 2014; Maiti and Tiwari, 2014; Alipour et al., 2014; Wen et al., 2015; Rezaei et al., 2017; Milan et al., 2018; Khosravi et al., 2018; Termeh et al., 2019; Chen et al., 2019; AlAyyash et al., 2023). Even though an ANFIS model has greater reliability compared to other mathematical models, finding the optimum intrinsic weight values of ANFIS is challenging given the constrained characteristics of the adaptive algorithm utilized (Bui et al., 2016; Heidari et al., 2019). To improve the predictability of groundwater models, this weighting should be improved using metaheuristic algorithmic optimization.

The objectives of this research are: (i) to obtain the lineament density through the superimposition of lineament maps from remote sensing, geological maps, and aeromagnetic data; (ii) to integrate the eight groundwater variable factors using ANFIS and optimize them with three different metaheuristic algorithms [Genetic Algorithm (GA), Particle Swarm Optimization (PSO), and Firefly Algorithm (FA)]; (iii) to verify the generated groundwater prediction models using well data. Following the most recent research, the evaluation of groundwater potential using ANFIS is unique to this region of the world. The study uses machine learning using ANFIS, which is enhanced by three metaheuristic algorithms, to progress the field. Eight predicting variables resulting from geophysical (electrical resistivity), aeromagnetic, and remote sensing approaches are extensively evaluated by this method. As a result, potential groundwater locations are defined exhaustively. This runs counter to the reality that the majority of academics only use machine learning algorithms with remote sensing techniques. This has the drawback that, due to low resolution and penetration depth, remote sensing cannot reliably anticipate the groundwater potential of an area. The final groundwater potential index using remote sensing is sometimes inaccurate because groundwater occurs at a depth that can't be detected by remote sensing, especially in a basement complex environment. As a consequence, the proposed methodology outlined in this study would be implemented in regions exhibiting similar groundwater conditions.

2 Study area

Ogbomoso of Southwest Nigeria is the location of the study area (Fig. 1). It is

situated between latitudes 08° 02ˈ50"N and 08°15ˈ15"N and longitudes 04°09ˈ50"E and 04°20ˈ45"E. The study area covers an area of approximately 441 km^2. The topographic elevation of the research area ranges from 303 to 368 m above mean sea level. Roads and pathways make it possible to reach the research area. The area under investigation is situated in the tropical rainforest belt of Southwest Nigeria. The rock units discovered at Ogbomoso are representative of the rocks found in Precambrian basement complex of Southwest Nigeria (Rahaman, 1976, 1988). According to NGSA (2010), the research region is underlain by migmatite gneiss, quartz diorite, quartzitic schist, and porphyroblastic schist (Fig. 2). A river that flows into the valleys on the northern border of the study area defines the area. With no systematic bifurcation of the tributaries, the drainage pattern is dendritic.

The research region is part of the Guinea Savannah Belt of Nigeria, but due to human-induced processes like deforestation, the vegetation is progressively transitioning to Sudan Savannah. The research area enjoys unusual tropical rains in the far southwest of Nigeria. The study region is dominated by the wet season, which typically lasts from March to October, and the dry season, which lasts from November to February.

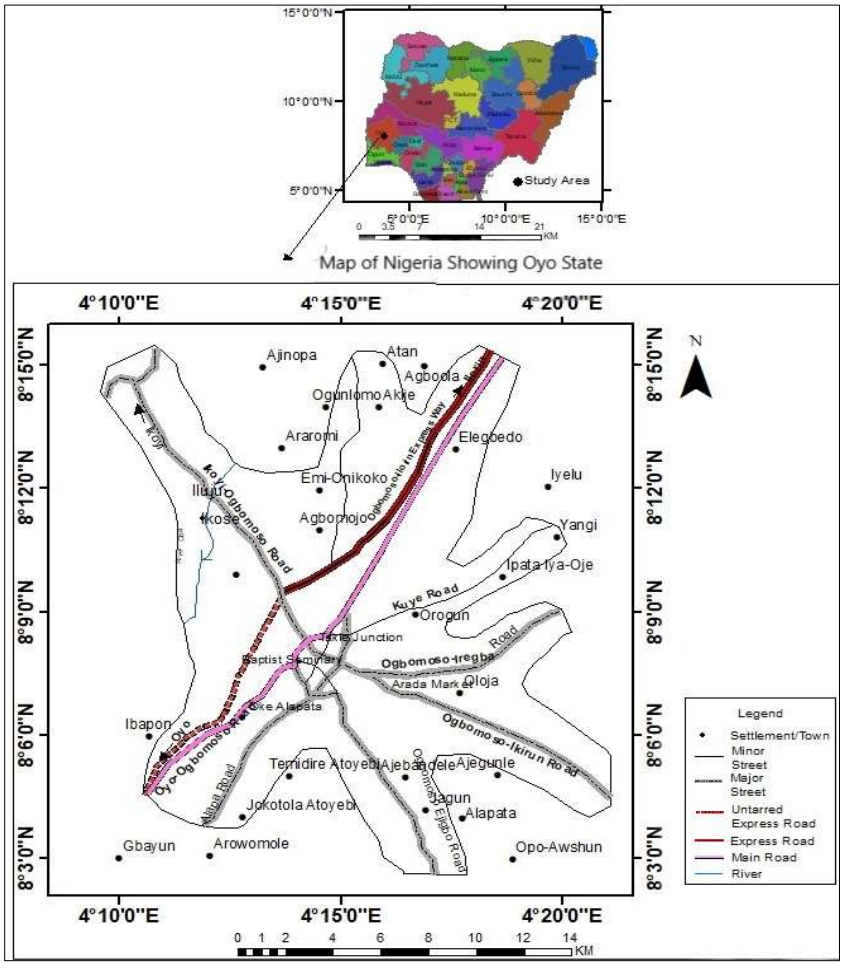

Figure 1. Map of the study area.

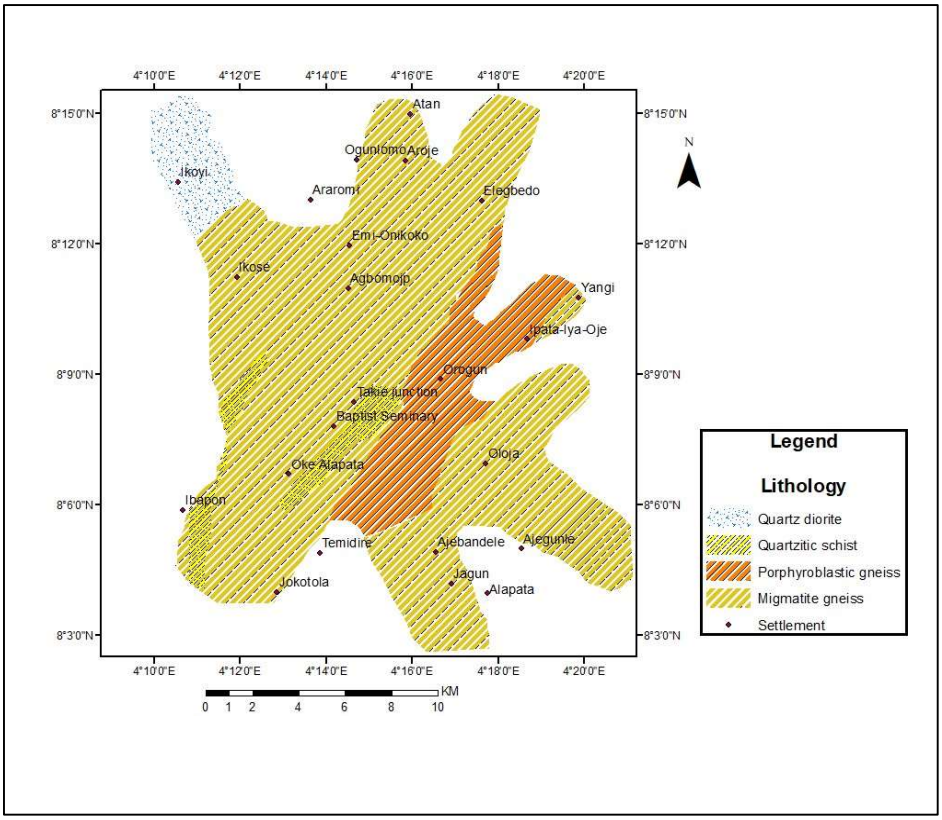

Figure 2. Simplified geological map of the study area [revised after NGSA (2010)].

3 Materials and methods

Remote sensing, aeromagnetic, geophysical (including electrical resistivity), and hydrogeological approaches were implemented in this study. Given its capacity to generate a huge dataset and diverse groundwater parameters, such as lineament, slope angle, and planar curvature, the remote sensing method has proven effective. A digital elevation model (DEM) with the coordinates of the study region was downloaded from the United States Geological Survey (USGS) through (https://asterweb.jpl.nasa.gov/gdem.asp, last access: November 20, 2019) with a spatial resolution of 15 m for this research endeavor. This was ingested directly into the ArcGIS 10.2 setting, where the slope map was created with the arctool box and the lineament map was produced from the images from Landsat. Edge improvement approaches were used to detect lineaments (Mah et al., 1995; Ozegin and Alile, 2021). These strategies generated edge maps that require additional processing (thresholding and thinning) for lineament sections to display with a one-pixel thickness (Akinlalu et al., 2018; Ozegin and Alile, 2023).

Additionally, the aeromagnetic data (Ogbomoso sheet 223 2009) was acquired from the Nigerian Geological Survey Agency (NGSA) between 2003 and 2009 underwent various aeromagnetic data optimization procedures, such as reduction-to-equator, near-surface noise filtering, residualization, and fast Fourier transformation using Oasis Montaj software. For the reduction-to-equator transformation, the declination and inclination parameters of ambient magnetic field were utilized. For near-surface noise filtering and residualization, an upward continuation filter came into play exclusively. The low wave number (long wavelength) abnormalities are amplified against the backdrop of the

high wave number anomalies through upward continuation. The magnetic field in this investigation was upward and persisted to a height of 3 km. To characterize geologic structure (lineaments) and anomaly depth, enhancement techniques, such as total horizontal derivative (THD), tilt derivative (TDR), tilt of total horizontal derivative (TDR_THD), and 3-D Euler deconvolution were used with residualized magnetic field intensity (RMI). In this study, the vertical electrical sounding (VES) technique and the Schlumberger ensemble were used in the electrical resistivity method. The electrode arrangement employed was from Schlumberger array with current electrode (AB) and potential electrode (MN) spacing of 1 to 120 m and 0.5 to 9 m, respectively. Fig. 3 shows the 165 VES stations established in the study area. A resistivity meter was used to measure the ground resistance. To determine the layer resistivity and thickness, computer iteration methods and manual curve matching were also used (Vander Velpen, 2004; Ilugbo et al., 2023b). Fig. 4 displays the typical VES curves collected from the research area. The resistivity type curves obtained in this area vary from 3 to 5-layer types. These include 3-layers (H and A), 4-layers (HA, QH, and KH), and 5-layers (HKH and AKH). The H-type is the dominant type curve in the study area, with the highest frequency of 93 and a percentage occurrence of 55%. The HKH, HA, QH, KH, AKH, and A type curves have frequency values of 20, 16, 16, 15, 3, and 2, respectively, while the percentage occurrences accounted for 13%, 10%, 10%, 9%, 2%, and 1%, respectively, of the total sounding curves. The resulting geoelectric characteristics were employed in the additional analysis of the study. In this research, the factors influencing groundwater potential were determined based on geophysical parameters. These factors were derived from both first-order geoelectric parameters and second-order geoelectric parameters (Dar-Zarrouk parameter), which are outlined in Eqs. (1–8):

$$H = h_1 + h_2 + h_3 + \cdots + h_n \quad (1)$$

where h is the thickness of each geoelectric layer and H is the total overburden thickness.

$$T = \sum_{i=1}^{n} h_i \rho_i = h_1 \rho_1 + h_2 \rho_2 + h_3 \rho_3 + \cdots + h_n \rho_n \quad (2)$$

T is the traverse resistance and ρ is the apparent resistivity.

$$S = \sum_{i=1}^{n} h_i p_i = \frac{h_1}{\rho_1} + \frac{h_2}{\rho_2} + \frac{h_3}{\rho_3} + \cdots + \frac{h_n}{\rho_n} \quad (3)$$

where S is longitudinal conductance.

The average longitudinal resistivity is:

$$p_L = \frac{H}{S} = \frac{\sum_{i=1}^{n} h_i}{\Sigma_{i=1}^{n} \frac{h_i}{\rho_i}} \quad (4)$$

The average transverse resistivity is:

$$p_T = \frac{T}{H} = \frac{\sum_{i=1}^{n} \frac{h_i}{p_i}}{\Sigma_{i=1}^{n} h_i} \quad (5)$$

and the coefficient of anisotropy (λ) is:

$$\lambda = \sqrt{\frac{p_T}{p_L}} = \sqrt{\frac{T/H}{H/S}} = \sqrt{\frac{T}{H} \times \frac{S}{H}} = \frac{\sqrt{TS}}{H} \quad (6)$$

$$K = 0.0538e^{-0.0072\rho} \quad (7)$$

where K is the hydraulic conductivity and ρ is the aquifer resistivity.

$$T = K \times H \quad (8)$$

where T is the transmissivity.

One hundred ten (110) hand-dug wells worth of data were collected to verify the model. The static water level (SWL), well depth, and coordinates for each well position make up this information. The 110 readily accessible hand-dug wells provided the basis for the static water level assessments throughout the study region. All of the available total depths of wells and static water levels were determined and noted. A heavy padlock was fastened to a measuring tape, and it was lowered to the bottom of each well to establish its total depth. This was done to calculate the saturation thickness of aquifers. Using Garmin GPSmap76Cx,

the coordinates of well locations were captured.

Depth to water table = EASL - SWL (9)

(10)

Saturated aquifer thickness=TWD -STA

where EASL is the elevation above sea level, STA is the saturated thickness of the aquifer, TWD is the total well depth, and SWL is the static water level.

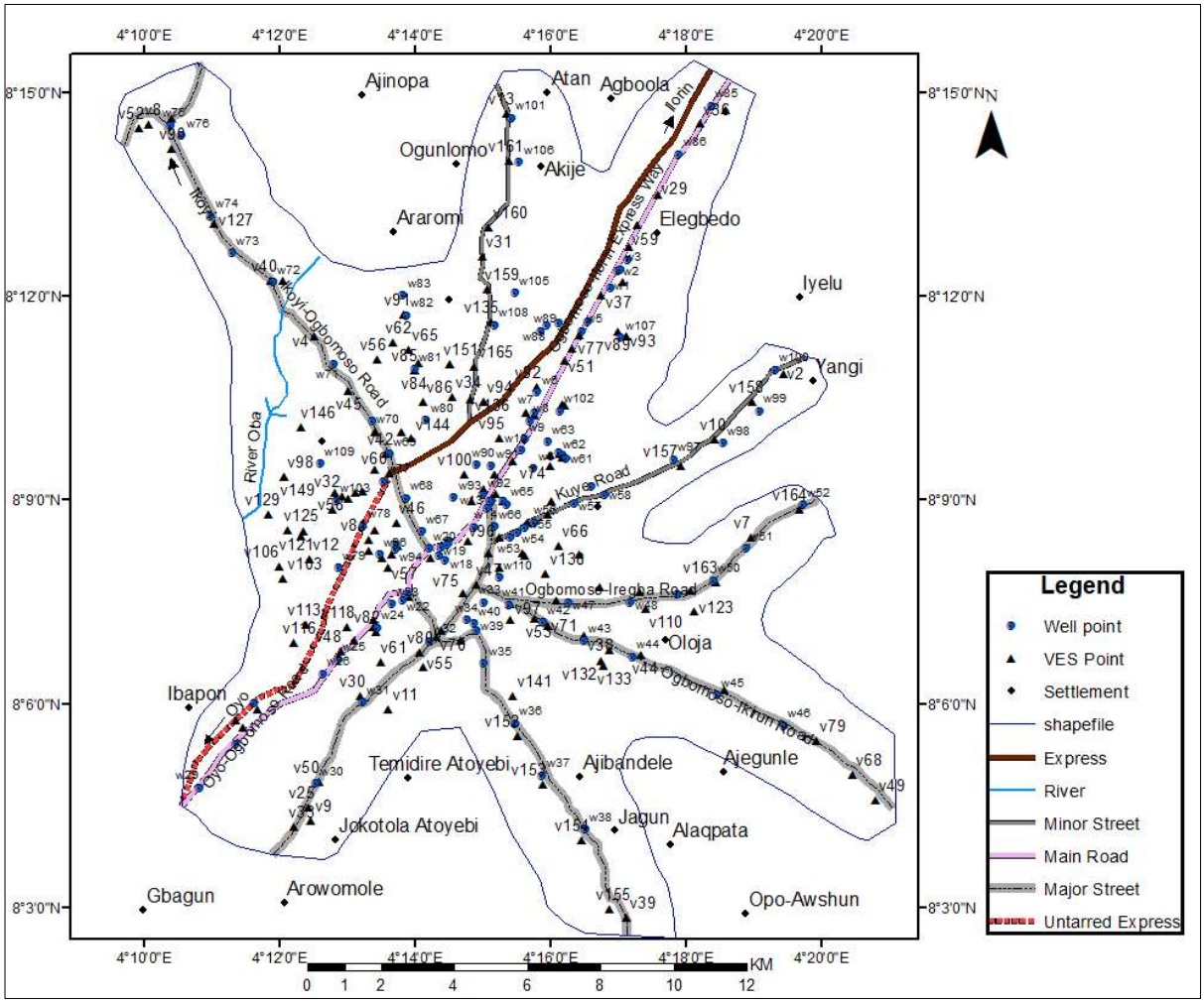

Figure 3. Data acquisition map for the research area.

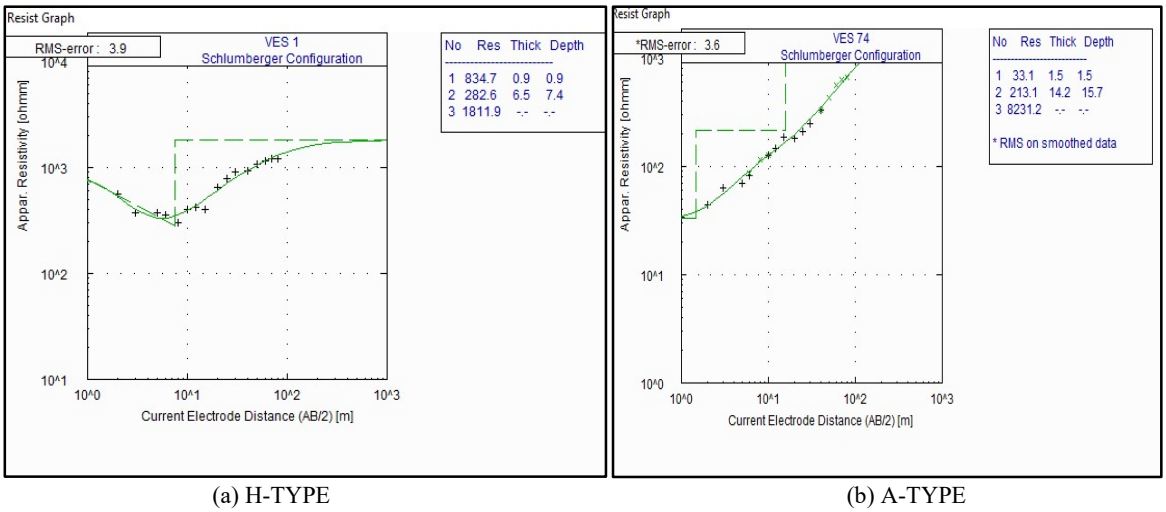

(a) H-TYPE (b) A-TYPE

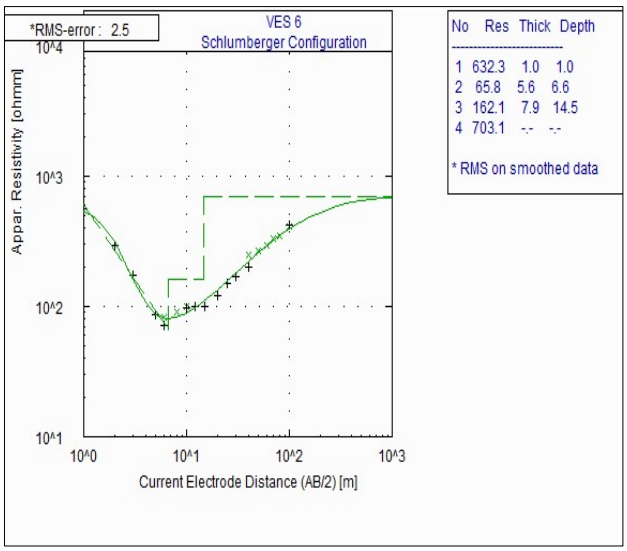

(c) HA-TYPE

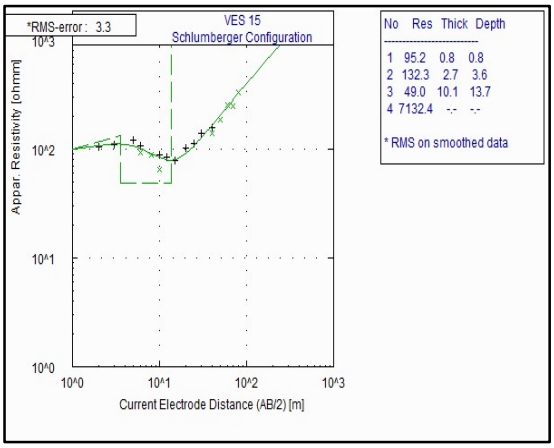

(d) KH-TYPE

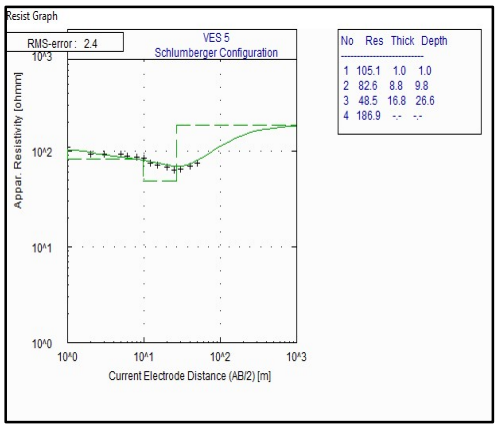

(e) QH-TYTPE

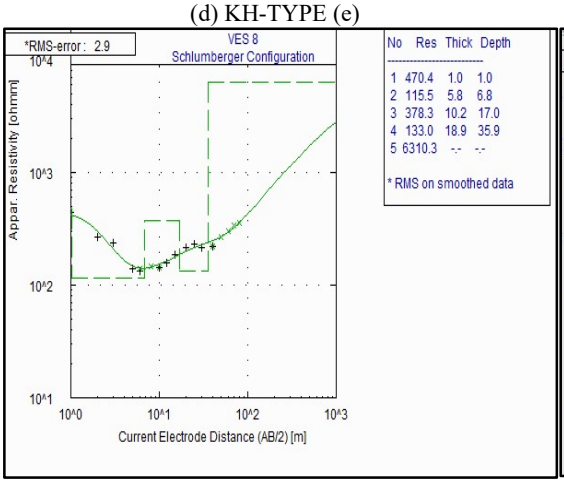

(f) HKH-TYPE

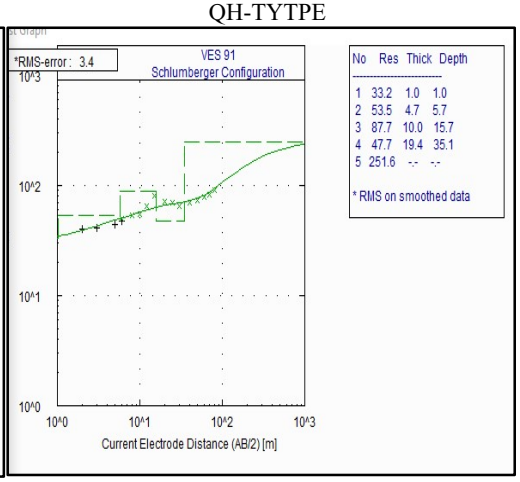

(g) AKH-TYPE

Figure 4. VES curves obtained from the study area.

3-1 Adaptive Neuro-Fuzzy Inference System

Contemporary structures are complicated and can be either nonlinear or linear, discontinuous or persistent, either static or dynamic (Mrinal, 2009). A mix of technologies termed the neuro-neuro-fuzzy inference system will be employed in an attempt to effectively manage the linear and non-linear character of the data

received from the study region. It combines fuzzy logic, which particularly addresses linearity in the data set, while the neural network focuses on non-linear data sets. Jang (1993) developed ANFIS to offer remedies for complicated issues in a single framework (Khabat et al., 2018). Artificial neural networks (ANN) and fuzzy logic (FL) are combined in ANFIS. A grouping function is used to transform the input data into fuzzy inputs in ANFIS. The various roles of membership are used to characterize the actions of the adaptive neuro-fuzzy inference system (Jang, 1993). ANFIS is utilized in the Takagi-Sugeno-Kang (TSK) fuzzy model, consisting of two "if-then" rules, both of which have a pair of inputs, X_1 and X_2, and one output, f (Takagi and Sugeno, 1985):

Rule 1: if x_2 is A_2 and x_2 is B_2;

then $f_2 = p_2x_2 + q_2x_2 + r_2$ (3)

Rule 2: if x_1 is A_1 and x_2 is B_1;

then $f_1 = p_1x_1 + q_1x_1 + r_1$ (4)

A_1, A_2, B_1, and B_2 are the functions that represent the membership of X_1 and X_2, and the output parameter values are p_1, q_1, r_1, p_2, q_2, and r_2.

3-2 Metaheuristic Optimization Algorithm

Though ANFIS is a strong framework with effective processing of complicated non-linear datasets, determining the optimal intrinsic weightings for ANFIS is challenging. This is due to the limitations of adaptive algorithm (Bui et al., 2016). As a result, these weights should be refined using a metaheuristic method. ANFIS has been optimized in this study using three metaheuristic algorithms: the genetic algorithm (GA), particle swarm optimization (PSO), and the firefly algorithm (FA). The three metaheuristic algorithms mentioned above were applied because prior research (e.g., AlAyyash et al., 2023; Khabat et al., 2018; Khosravi, et al. 2018) had demonstrated their efficacy in the optimization of groundwater parameter variables.

3-2-1 Genetic Algorithm

Natural selection, the mechanism that causes biological evolution, is handled by genetic algorithms in both restricted and unbounded nonlinear optimization issues.

3-2-2 Particle Swarm Optimization

Particle swarm optimization (PSO) is a population-centered optimizing algorithm driven by how birds employ collaborative intelligence to discover the most suitable route to gather food (Kennedy and Eberhart, 1995).

3-2-3 Firefly Algorithm

The Firefly technique of Yang (2009) is a nature-inspired optimization strategy based on the flashing behavior of fireflies. This algorithm is used to solve optimization and search challenges. It's particularly ideally suited to continually improving challenges. The fundamental concept underpinning the firefly algorithm is to use the flashing patterns created by fireflies to assist in the search for an ideal solution in a multifaceted search space.

3-3 Construction of the training and testing datasets

Constructing training and testing datasets is a critical stage in machine learning for assessing and certifying the effectiveness of a model. Two classes were randomly chosen from the groundwater-influencing variable dataset. 30% of the data collection was employed for testing, and the remaining 70% was used for training. The ANFIS model, which is substantially connected to numerous system recognition methods, is depicted in Fig. 5. The hypothetical parameters of model structure are first set. The input data is gathered in a format that ANFIS can use for instructions. The input data is modeled using fuzzy functions for

membership by ANFIS. It's necessary to initialize these functions of membership. These functions frequently take the Gaussian, triangular, and bell shapes. ANFIS computes each rule output during the forward pass and integrates it with other rule outputs to create the model output. Additionally, a back propagation process will be engaged to modify the ANFIS model variables to reduce the prediction error. The testing datasets will be utilized for validating the model.

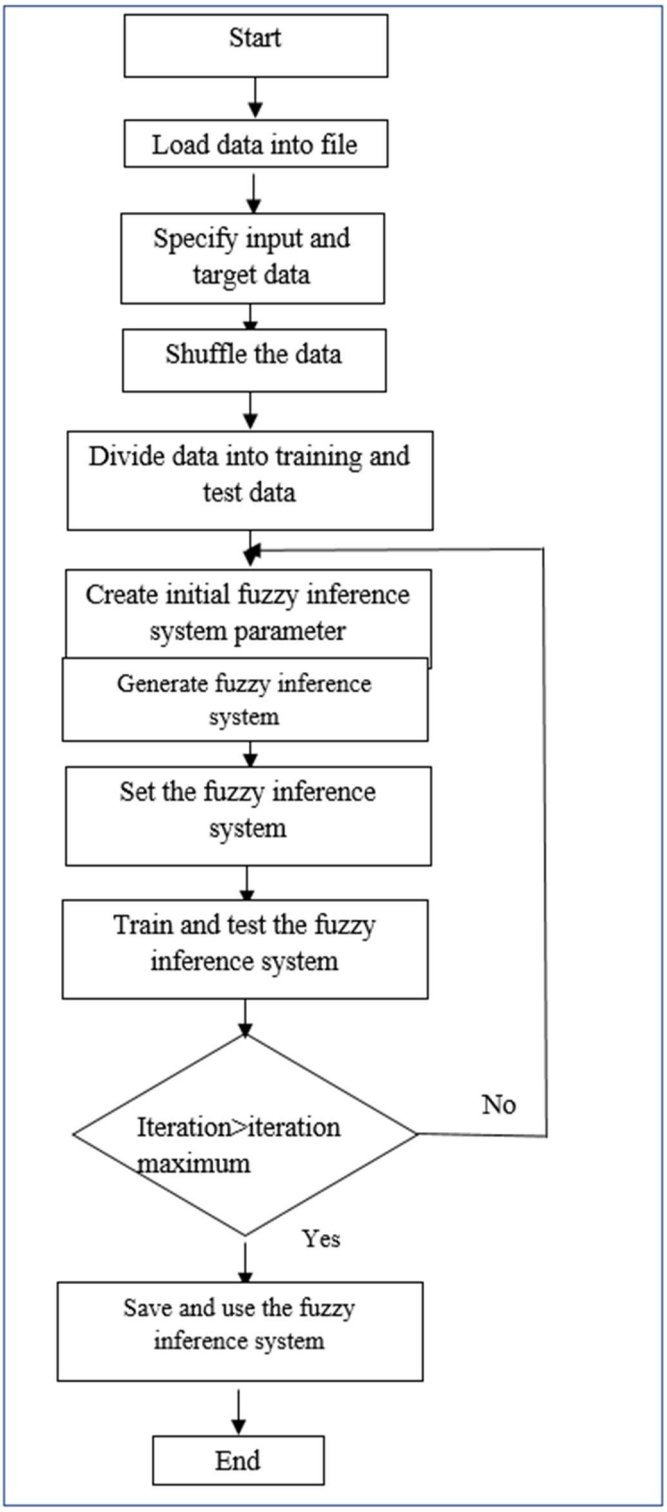

Figure 5. Schematic diagram for the ANFIS model.

3-4 Validation

A model must be validated to be evaluated for performance and dependability. A linear correlation technique is employed to validate this model. To find the most accurate predictive model, the groundwater potential indices and water column thicknesses are linearly connected.

4 Results and discussion

4-1 Groundwater factors influencing groundwater potential in the study area

4-1-1 Slope

Huajie et al. (2016) assert that groundwater flows are driven by surface forces, and the boundaries of the shallow aquifer are typically the boundaries of the topography. Fig. 6a presents the slope angle map from remote sensing data. The elevation at each location is used to calculate the angle of raster cell on the map. The slope degrees extracted from the DEM of the study area were divided into five categories using the ArcGIS tool. They are classified as 0-1.80º, 1.80º-3.07º, 3.07º-4.35º, 4.35º-5.98º, and 5.98º-14.81º, which have a percentage contribution of 15%, 13%, 19%, 30%, and 23%, respectively, of the total landmass of the investigation area. Areas with a high slope angle will have low groundwater potential because of runoff, while areas with a low slope angle will have high groundwater potential because of their ability to retain groundwater (e.g., Ozegin et al., 2023; Ilugbo et al., 2023a). The different classes are represented by different color ramps in Fig. 6a.

4-1-2 Lineament Density (LD)

The TMI map of the research area (Fig. 6b) was shown as a color-shaded relief map. Magnetic anomaly measurements identified in the study area vary from -54.7 to 94 nT. The broad spectrum of numbers reflects differing varieties of rocks in the basement complexities of research area (e.g., Ozegin and Alile, 2023). On the geological map, the considerably low magnetic intensity values in the range of -54.7–33.5 nT established in the southeastern, central, and sections of the study area correspond with the quartzitic schist in the central part of the investigation area and the migmatite gneiss in the southeastern part of the study area. A low/negative magnetic peak value shows typical abnormal patterns that define faults and fracture zones in a low-latitude magnetic region, notably around the equator, where Nigeria is located (Parasnis, 1986; Ozegin and Alile, 2021).

To obtain the lineament map of the study area, the TMI map was subjected to various optimizing and filtering methods, such as reduction to the equator (RE), residual magnetic intensity (RMI), total horizontal derivatives (THD), tilt derivatives (TD), and Euler deconvolution (ED), as shown in Fig. 6c. This is advantageous to the area of potential groundwater supply and consequently improves the likelihood of groundwater production (Akinluyi et al., 2021; Ilugbo et al. 2023a). Fig. 6d highlights the LD map of the study area. Lineaments from remote sensing maps, aeromagnetic maps, and geological maps were superimposed. The lineament density of an area is defined as the ratio of the overall length of the complete lineament observed to the area under consideration (Edet et al., 1998). The values of the lineament density for the study area generally range from 0.0 to 352.96 km/km². The generated lineament density value of the investigation area was classified into very low (0–26.29 km/km²), low (26.29–73.36 km/km²), moderate (73.36–131.49 km/km²), high (131.49–218.70 km/km²) and very high (218.70–352.96 km/km²). The areas that are characterized by very low and low values

occupy a large part, which is found to be distributed in all parts of the study area. The moderate values are found to be distributed across the entire study area. The high class values and the very high values are found to cover a small isolated area located in the northeast, southwest, and northeastern area of the study area. The majority of the lineaments are observed to trend in the NE-SW direction. Hard rock hydrogeology places a great deal of emphasis on lineaments since they can be used to locate groundwater-containing rock fractures (Honore et al., 2013; Ozegin and Alile, 2021; Ozegin and Alile, 2023; Ilugbo et al., 2023b).

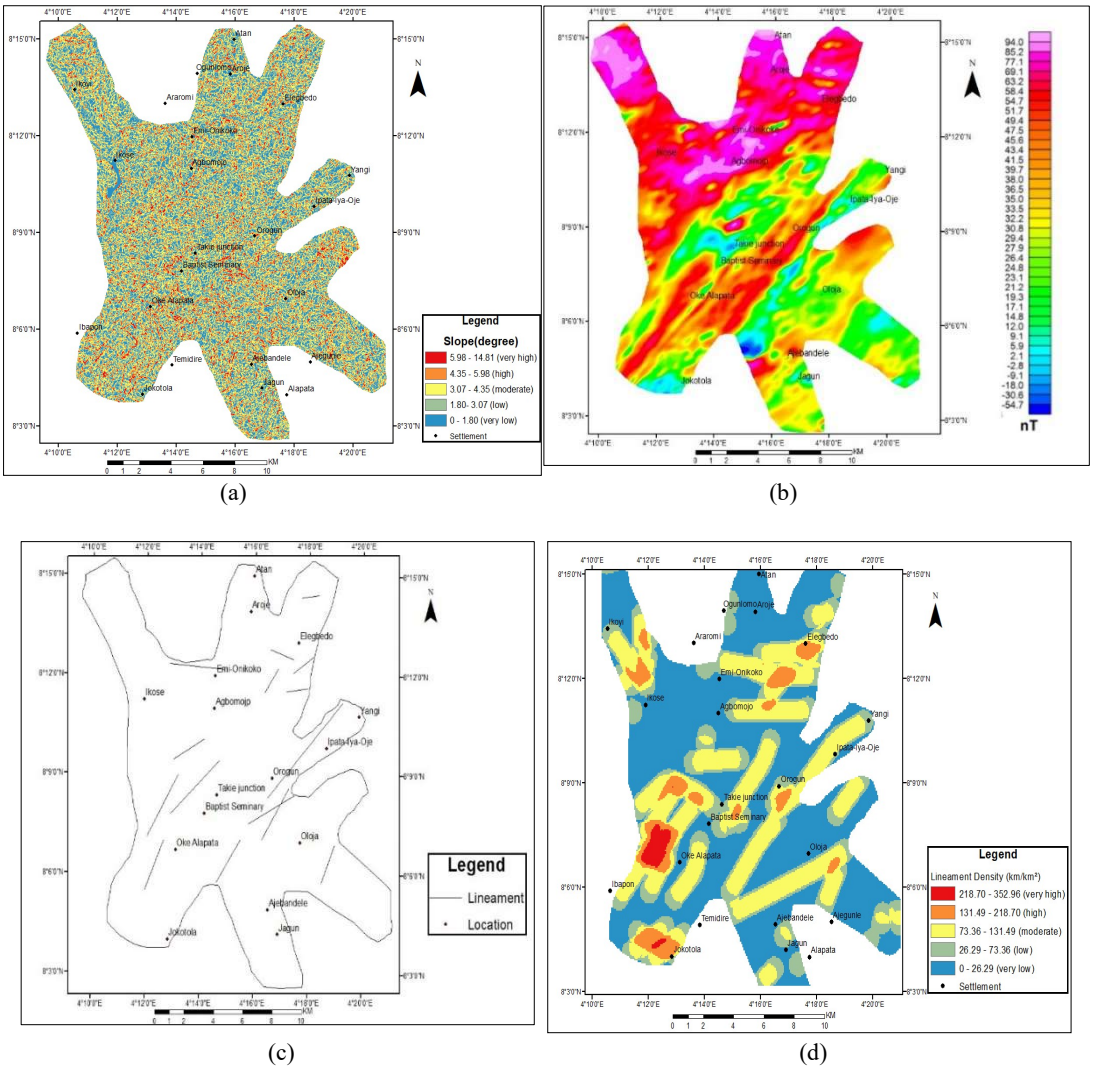

(a) (b)

(c) (d)

Figure 6. (a) Slope map of the study area (b) Total magnetic intensity (TMI) map in the study area (c) Lineament map from aeromagnetic data of the study area (d) Lineament density of the study area.

4-1-3 Lithology

The lithology of a rock unit explains the physical properties of an exposure in a core, hand sample, or under minimal magnification microscopy. According to Huajie et al. (2016), lithology significantly impacts on the ability of aquifer to retain water, which consequently impacts the presence and dispersion of groundwater. The geologic map from the NGSA was used to create the theme lithology map (Fig. 7a). The map reveals four different rock types: migmatite gneiss, porphyroblastic gneiss, quarzitic schist, and quartz diorite. The migmatite gneiss rock unit is the parent and the oldest rock that

dominates the study area. The porphyroblastic gneiss is present in the central part of the study area and the quartzitic schist occurs as an intrusion within the migmatite gneiss in the central and southwestern parts of the study area. The quartz diorite occurs in the northwestern part of the study area. The percentage occurrences of the lithologic units of migmatite gneiss, porphyroblastic gneiss, quartzitic schist, and quartz diorite are 80%, 10%, 7%, and 3%, respectively, of the total land mass of the study area (Fig. 7b). Quartzite schist zones are highly weathered zones, which implies that the region will have high groundwater potential, while other areas will depend on secondary fracturing for moderate to high groundwater potential (Ilugbo et al., 2023a).

4-1-4 Map of the overburden layer

Fig. 7c presents the overburden thickness map for the investigation area. The values of the overburden thickness in the study area generally range from 3.1–76.3 m, with a mean value of 19.4 m. This was classified into very low (3.1–14.3 m), low (14.3–21.2 m), medium (21.2–30.1 m), high (30.1–43.9 m), and very high (43.9–76.3 m) overburden thickness values using the natural break method of classification in ArcMap 10.2. The very low and low thickness classes occupied major portions of the northern, western, southwestern, southeastern of the region, and portions of the central part of the study area. The moderate thickness class is found to be distributed across the central and southern parts of the study area. The high and very high overburden thickness values are found in the southwest and central parts, with pockets of occurrence in the northern parts of the study area. Groundwater potential is projected to be significant in areas with a low percentage of clay, heavy overburden thickness, and considerable inter-granular flow, particularly in the basement complex areas (Okhue and Olorunfemi, 1991). Also, the cardinal focus on group assessment in the crystalline rock area is where the overburden and fractured basement aquifers are complementary or connected (Bayode et al., 2011; Mogaji *et al.,* 2011). Moreover, the weathered layer, the partly weathered/fractured basement, and the fractured basement constitute the major aquifer unit with significant hydrogeologic importance within the study area. Therefore, the zones that are characterized by medium, high, and very high overburden thickness values can be considered prospective zones for the possible location of boreholes in the study area.

4-1-5 Bedrock relief

The bedrock map generated for the investigation area (Fig. 7d) was classified into very low (139.1–289.0 m), low (289.0–316.6 m), medium (316.6–333.3 m), high (333.3–353.1 m), and very high (353.1–390.5 m) bedrock relief zones. The areas that are characterized by very low and low values of bedrock relief are found to occupy the southwest, west, central, and north-central parts of the study area. Areas that are characterized by moderate bedrock relief are found to occupy the southern, western, central, and northwestern parts of the investigation area, while high and very high bedrock relief values are found in the northwestern, northeastern, eastern, and southeastern parts of the study area. The bedrock relief values that are characterized by high and very high are considered to be the ridges, hence the groundwater radiating zones. These values are adjudged to be of low groundwater potential zones. The moderate zones are considered to be located along the slope of the basement ridges. However, the very low and low zones are considered to be the basement depression zones, hence groundwater collecting centers. These zones are

considered to be the high groundwater potential zones. The hydrogeologic relevance of the bedrock relief has been recognized by Olorunfemi and Olorunniwo (1985), Dan-Hassan and Olorunfemi (1999), Omosuyi *et al.* (2003), and Bayode (2018). According to Adiat et al. (2009) and Bayode (2018), depression-characterized places have heavy overburdens, whereas ridge-characterized areas have slim overburdens. Basement depressions form groundwater collecting centers, especially water displaced from ridges. It is then expected that areas identified as depression zones in the map are the groundwater collection centers and are expected to play a significant role in groundwater development in the study area and typical basement complex terrain. Therefore, the basement depressions are considered to have higher groundwater potential than the basement ridges in the investigation area.

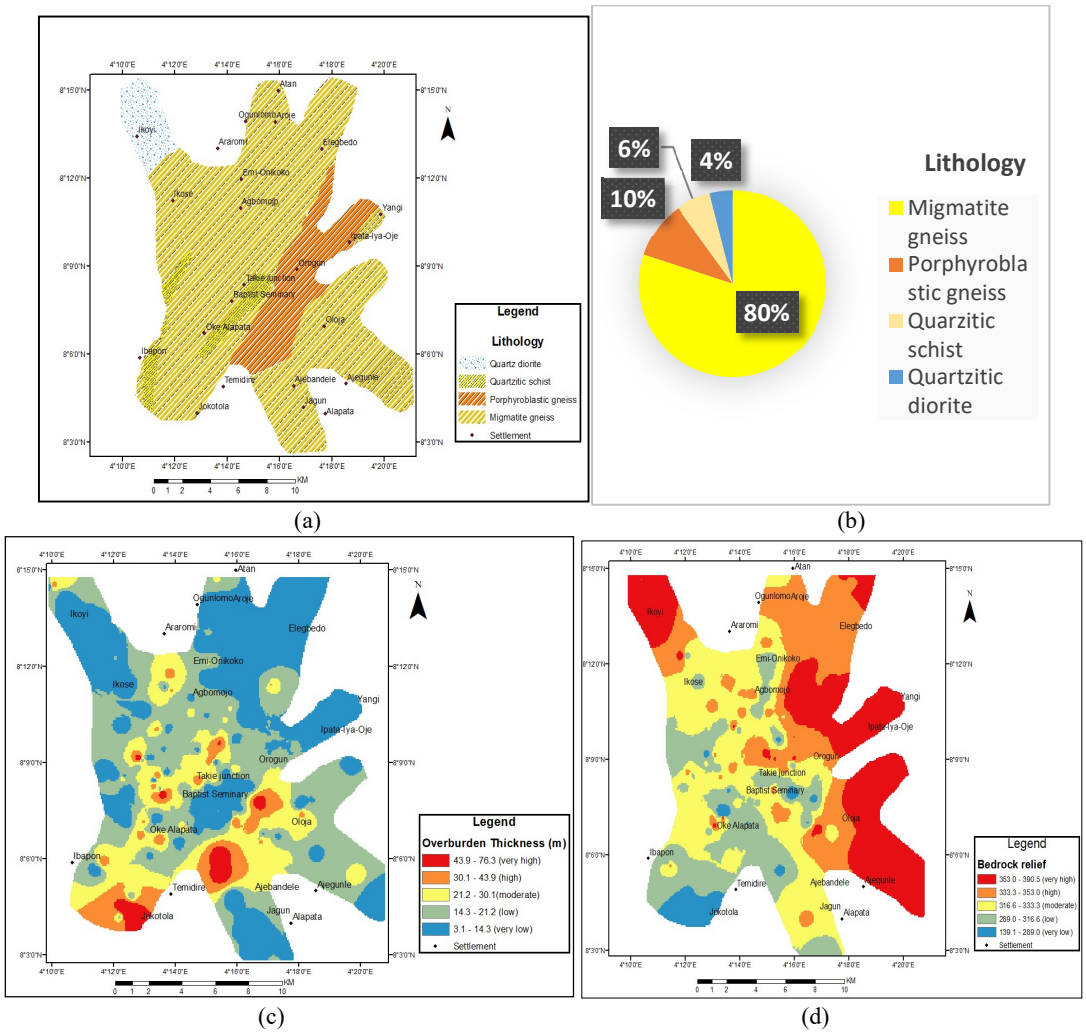

Figure 7. (a) Lithology map of the study area (b) Pie chart showing the percentages of the lithology (c) Overburden thickness map of the study area (d) Bedrock relief map of the study area.

4-1-6 Coefficient of anisotropy (λ)

The coefficient of anisotropy (λ) values obtained for the investigation area, as presented in Fig. 8a, generally vary from 0.49 to 3.49 with a mean value of 1.27. The coefficient of anisotropy generated for the investigation area was classified as very low (0.49–1.14), low (1.14–1.21), moderate (1.21–1.29), high (1.29–1.41), and very high (1.41–3.49). The areas that are characterized by very low and low values of λ are found to occupy primarily

the central and southern parts of the study area, while pockets of small areas are found in the northwestern and southwestern parts of the investigation area. The moderate values are found to be distributed across the entire study area. The high and the very high values are found to cover the east, west, northeast, south, and southeast, with pockets of occurrence in the central part of the study area. Although the geology of the study area is not mono-lithologic but predominantly migmatite gneiss, based on this, the inhomogeneity in the value of the coefficient of anisotropy could be attributed to variance in the thickness of the weathered layer material of the different geologic units.

Additionally, the groundwater potential declines and the coefficient of anisotropy increases as rock compactness and hardness rise (Keller and Frischknecht, 1966; Keary and Brooks, 2002). Areas that are characterized by very low and low values of λ are classified as high groundwater potential zones, while areas with moderate, high, and very high values are classified as poor groundwater potential zones.

4-1-7 Hydraulic conductivity

Fig. 8b shows the hydraulic conductivity map of the investigation area. A characteristic of porous materials, such as soil or rock, for transporting water through them is referred to as hydraulic conductivity. The hydraulic conductivity values obtained for the investigation area generally vary from 0.05 to 2.28 m/day, with a mean value of 1.27 m/day. The hydraulic conductivity generated for the investigation area was classified as very low (0.05–0.07 m/day), low (0.07–0.09 m/day), moderate (0.09–0.12 m/day), high (0.12–0.21 m/day), and very high (0.21–2.28 m/day). The areas that are characterized by very low and low values of hydraulic conductivity are found to occupy the west, northwest, northeast central, and a small portion in the southern segment of the investigation area. The moderate values are found to be distributed across the entire study area. The high and the very high values of hydraulic conductivity are also found to cover a small isolated area located in the north, north-central, east, central, and southwestern parts of the study area. According to Adeniji et al. (2017) and Ozegin et al. (2024), areas with high hydraulic conductivity are most likely to possess good aquifer recharge quality; hence the high and very high values of hydraulic conductivity constitute the high groundwater potential zones in the study area.

4-1-8 Transmissivity

The measured values of transmissivity determined for the area under investigation typically span from 0.18 to 39.88 m²/day, with an average value of 2.28 m²/day (Fig. 8c). The transmissivity map generated for the investigation area was classified into very low (0.18–0.80 m²/day), low (0.80–1.27 m²/day), moderate (1.27–1.74 m^2/day), high (1.74–3.14 m²/day) and very high (3.14–39.88 m²/day). The areas that are characterized by very low and low values are found to occupy the northeast, northwest, west, central, and pockets of occurrence in the southeastern parts of the study. The moderate values of hydraulic conductivity are distributed across the entire study area. The high and the very high values of transmissivity are also found in the north, south, southwest, north-central, and pockets of small occurrence in the southeastern component of the study region. Generally, groundwater yield increases with an increase in the value of transmissivity. Transmissivity is a significant variable in characterizing rocks as a water conductivity media (Fatoba et al., 2014; Ozegin et al., 2024). This can be attributed to an increase in porosity and

permeability with thickness. Hence, areas that are characterized by moderate, high and very high values of transmissivity are classified as moderate to high groundwater potential zones, while areas with very low and low values of transmissivity are classified as low groundwater potential zones. The hydraulic conductivity and transmissivity maps obtained from the investigation area are found to have a good correlation.

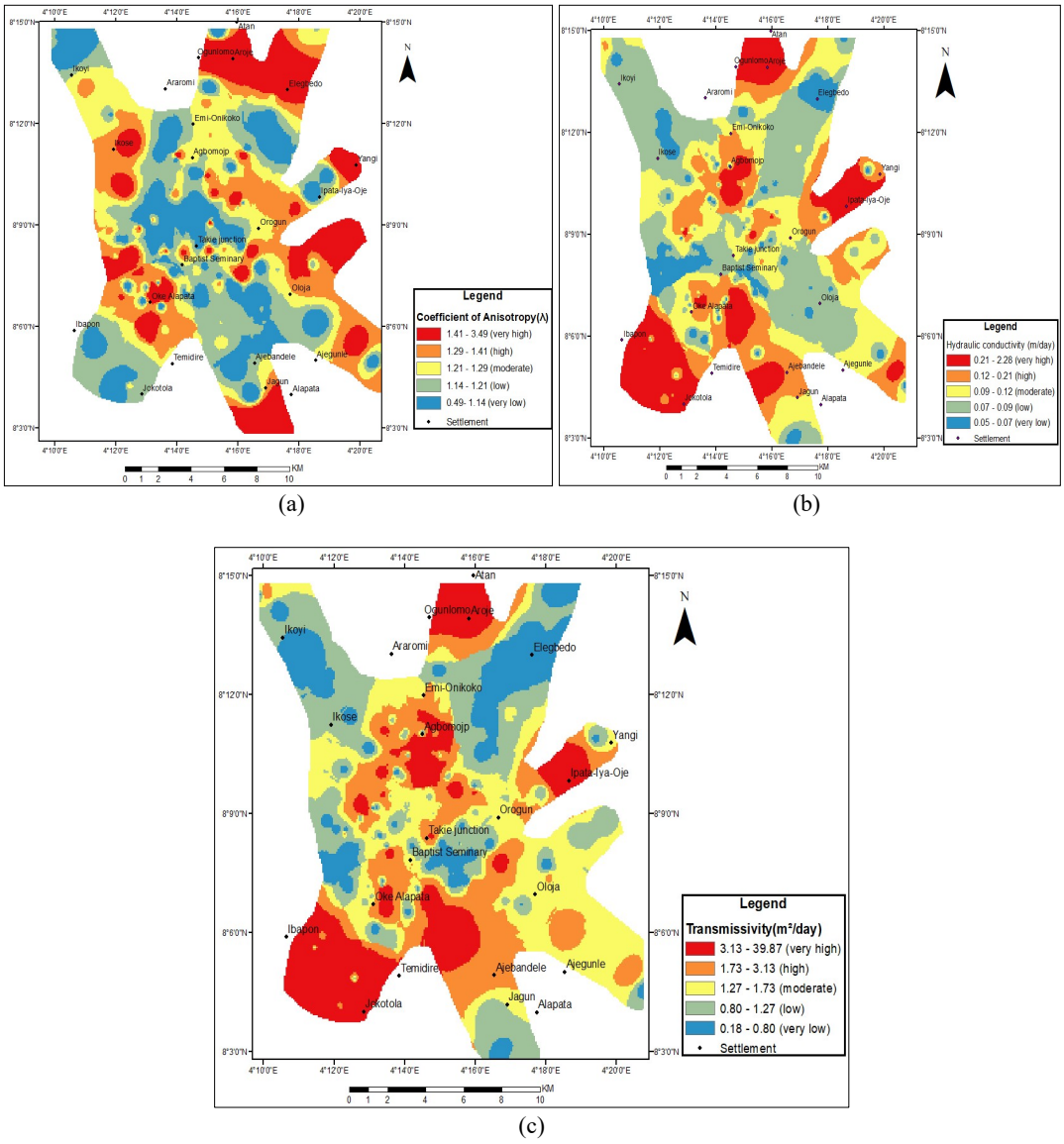

(a) (b)

(c)

Figure 8. (a) Coefficient of anisotropy map of the study area (b) Hydraulic conductivity map of the study area (c) Transmissivity map of the study area.

4-2 Application of ANFIS ensemble models

The ANFIS information from the training (Table 1) shows that 294 nodes were generated during the deep neural network**.** **The** linear and nonlinear parameters, which are the patterns found during the training of the dataset, are 1024 and 24, respectively. The total number of fuzzy inference system (FIS) parameters is 1066. The total number of training data pairs and fuzzy rules is 115 and 128, respectively, while the number of checking data pairs is zero. Fig. 9 shows the ANFIS-GA, ANFIS-PSO, and ANFIS-FA models using the training

dataset. The root mean square error (RMSE) values of the ANFIS-GA, ANFIS-PSO, and ANFIS-FA models are 0.0072232, 0.0077855, and 0.011097, respectively. This shows that the ANFIS-GA model has the lowest error value during the course of training the dataset, whereas the ANFIS-FA model has the highest RMSE value of 0.011097. The ANFIS-GA also has the lowest standard deviation error value of 0.20683, while the ANFIS-FA has the highest at 0.31779.

Fig. 10 depicts the prediction performance of the three models using the testing dataset. The ANFIS-GA, ANFIS-PSO, and ANFIS-FA models have RMSE values of 0.0095917, 0.0097023, and 0.0112748, respectively. This also means that the ANFIS-GA has the lowest error rate when testing the accuracy of trained models. However, the execution speeds of the three models were shown to be quite significant in addition to accuracy. The running time for 1000 iterations was approximated to determine this.

Fig. 11 depicts the outcome. Running times for the ANFIS-GA, ANFIS-PSO, and ANFIS-FA models were 107.28, 103.07, and 1053.70 seconds, respectively. The ANFIS-PSO model had the shortest data processing running time, which meant it trained quicker than the ANFIS-GA and ANFIS-FA models, while the ANFIS-FA model had the longest. On the contrary, it is possible to demonstrate how each model achieves learning convergence.

A convergence graph for all three models was generated using the cost function values, as illustrated in Fig. 12. The convergence process is depicted in Fig. 12a as a smooth curve with a rapid drop at the start and a steady slowdown at the 300th iteration. Fig. 12b depicts the convergence phase, which begins with a rapid reduction and continues until the iteration is completed. Fig. 12c depicts the point of convergence of a smooth curve with a rapid decline at the beginning and an unvarying procedure from the 90th iteration to the finish. The early strong drop of the Firefly algorithm in the optimization metric indicates rapid learning, which could indicate or not indicate good accuracy. It can simply represent the dataset underfitting.

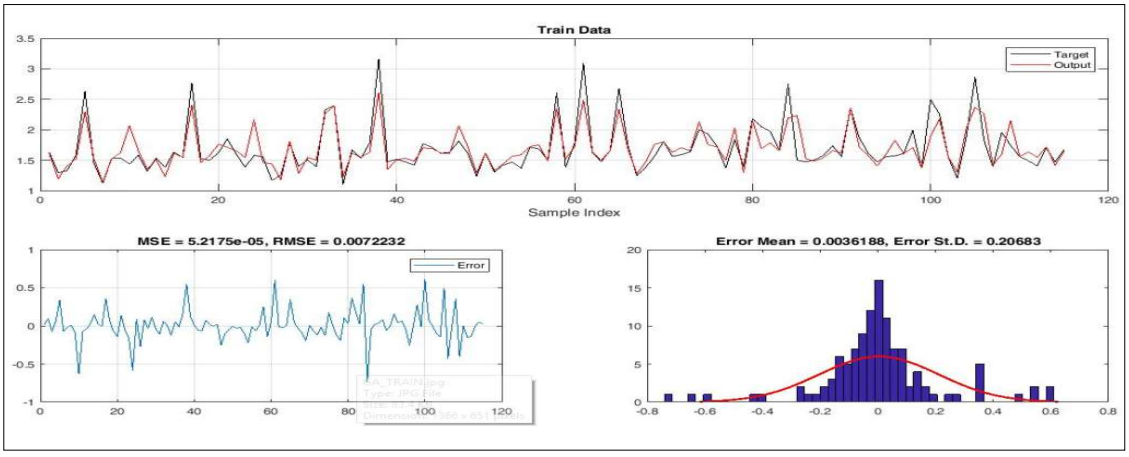

(a)

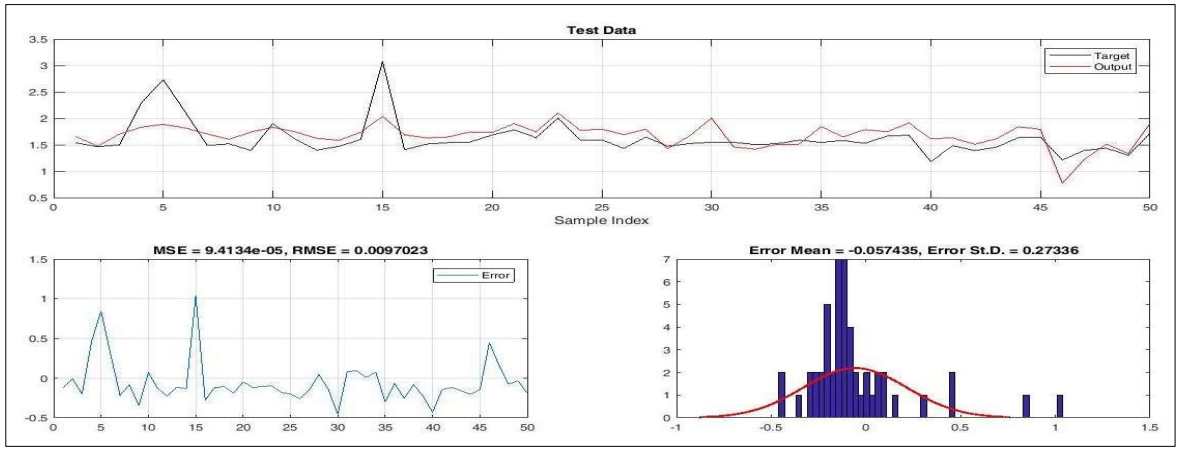

(b)

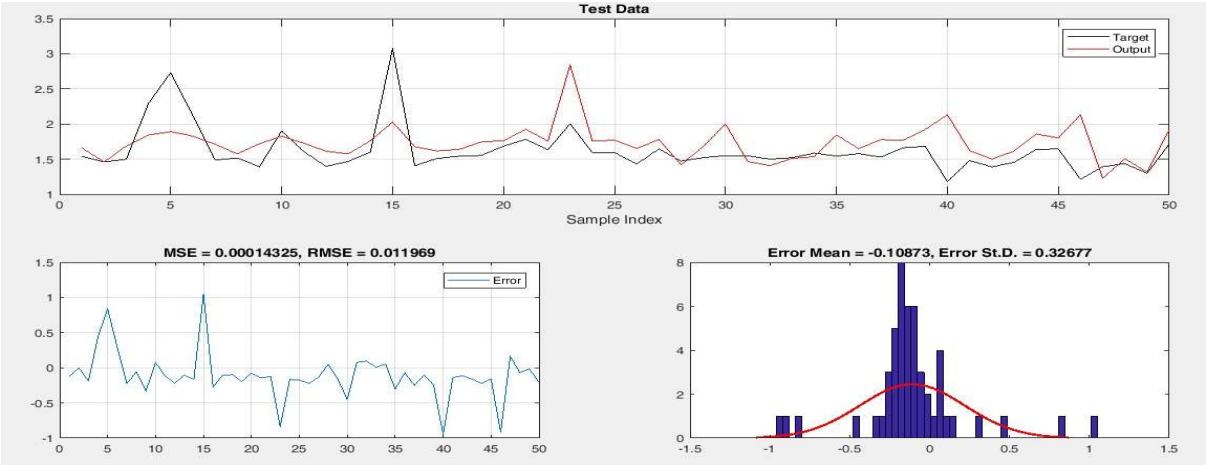

(c)

Figure 9. (a) MSE and RMSE values of ANFIS-GA models using the training dataset (b) MSE and RMSE values of ANFIS-PSO models using the training dataset (c) MSE and RMSE values of ANFIS-FA models using the training dataset.

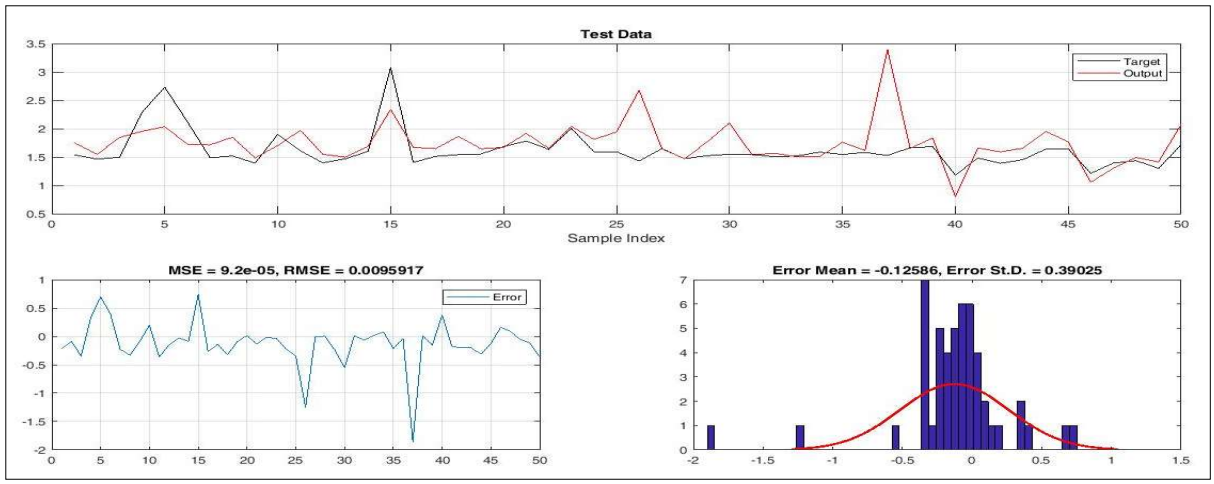

(a)

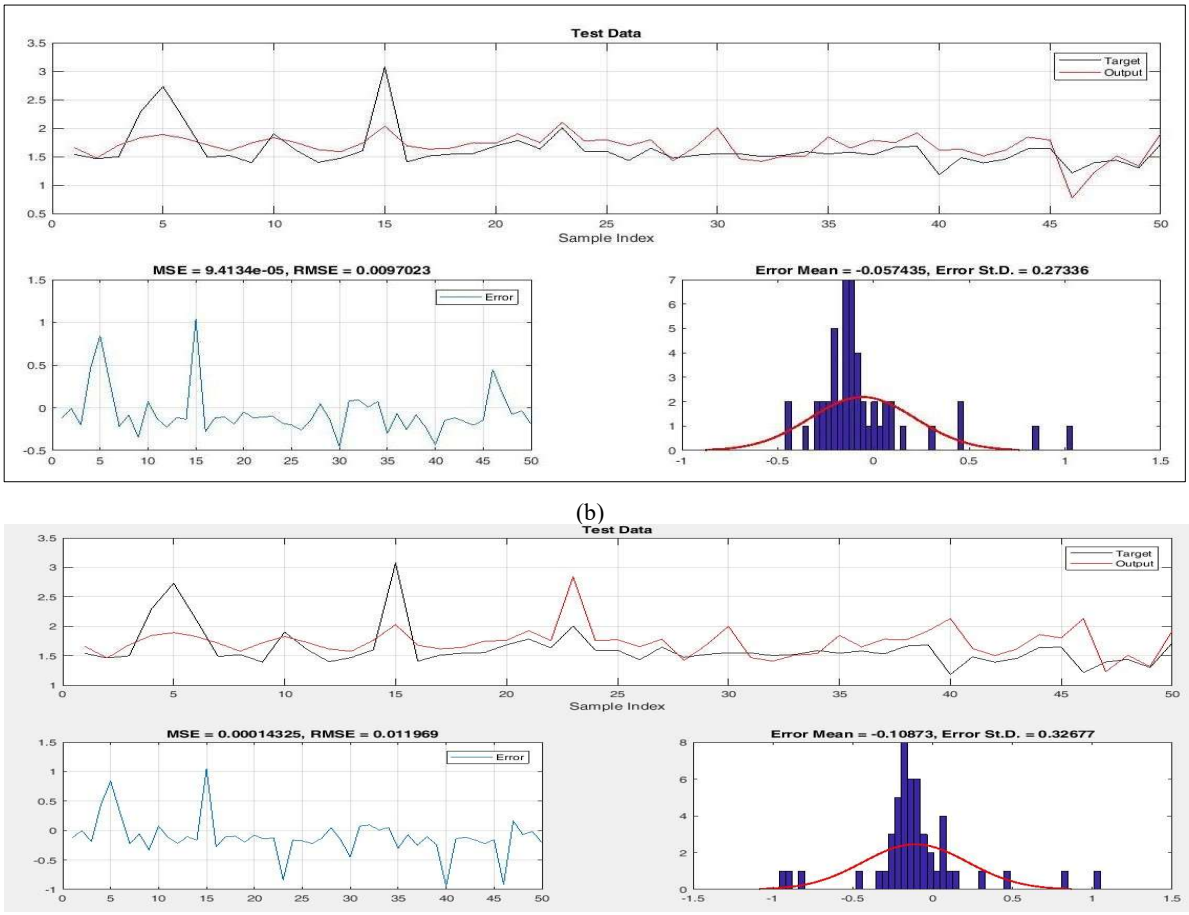

Figure 10. (a) MSE and RMSE values of ANFIS-GA models using the testing dataset (b) MSE and RMSE values of ANFIS-PSO models using the testing dataset (c) MSE and RMSE values of ANFIS-FA models using the testing dataset.

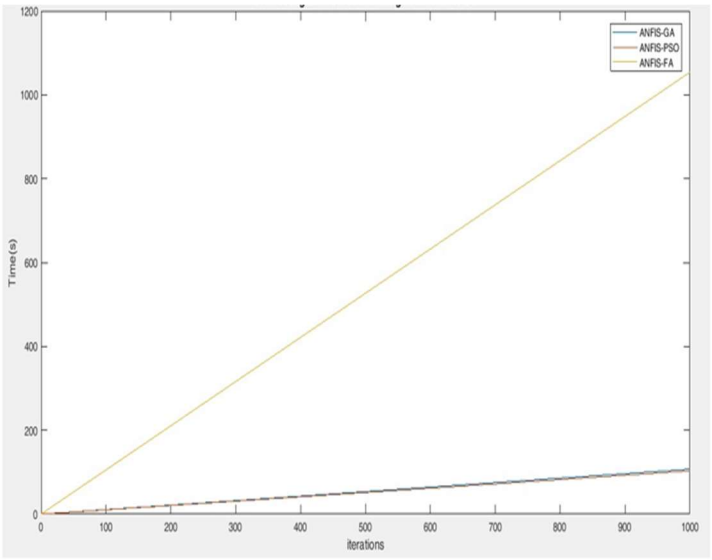

Figure 11. Processing time used for training the three models.

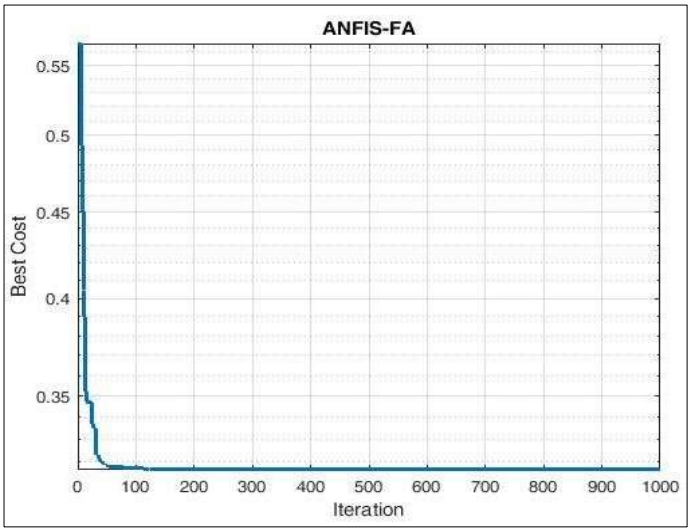

(a)

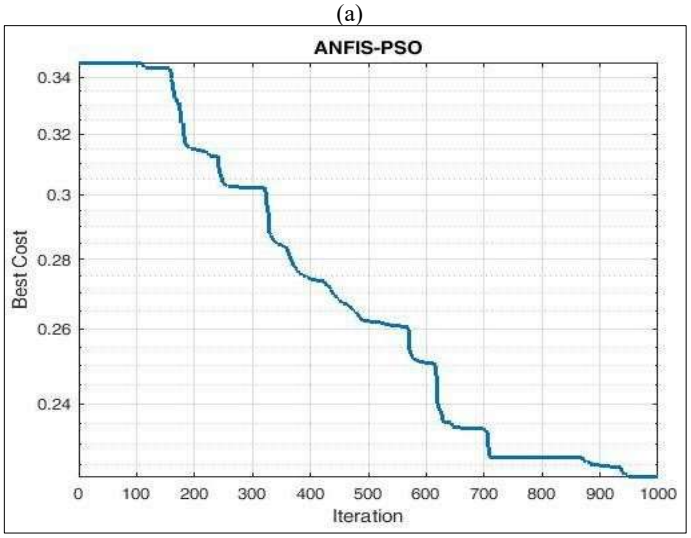

(b)

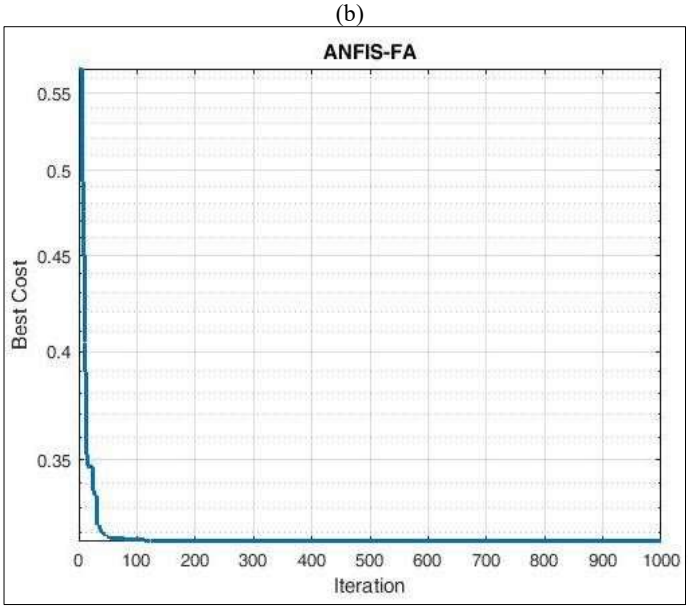

(c)

Figure 12. (a) Evolving optimal ANFIS value using GA (b) Evolving optimal ANFIS value using PSO (c) Evolving optimal ANFIS value using FA.

Table 1. The ANFIS information.

ANFIS information	
No. of nodes	294
Quantity of linear variables	1024
Quantity of nonlinear variables	24
Overall No. of parameters	1066
No. of training data pairs	115
No. of checking data pairs	0
No. of fuzzy rules	128
Minimal training RMSE	0.022160

4-3 Groundwater potential maps generated with ANFIS hybrid models

The models that have been effectively trained and examined were implemented for calculating groundwater potential indices for all of the VES locations in the studied areas. The indices, based on the final weight established using training the dataset, were transmitted from MATLAB into ArcGIS 10.2 software for establishing the groundwater potential map (Fig. 13) of the research area. Using the quantile approach, the resulting maps were classified into three classes: low, moderate, and high. The method of classification is determined by the distribution and categorization of groundwater spring indicators in a histogram (Ayalew and Yamagishi, 2005). The east, southeast, and north-eastern regions of the groundwater potential map (Fig. 13a), created using ANFIS-GA, display a low groundwater potential index ranging from 0.77 to 1.63. In the western portion and other regions of the analyzed area, there are several isolated areas with a low groundwater potential index. With an index ranging from 1.63 to 1.74, the identified groundwater potential index is moderate throughout the north-central, central, northwestern, southwestern, and part-southeastern regions of the study area. The groundwater potential index is found to be high in a significant percentage of the research area, ranging from 1.74 to 2.50 in the north-central, central, southwestern, and southern regions.

The east, southeast, north-eastern, and isolated areas in the western part of the research region have low groundwater potential index values that range from 0.77 to 1.63, according to the groundwater potential map (Fig. 13b) created using ANFIS-PSO. In the north-central, central, north-west, and south-western regions of the research area, the groundwater potential index is moderate, with groundwater index values ranging from 1.63 to 1.74. The research area has high groundwater potential index values that range from 1.74 to 2.50 in a significant portion of the north-central, southwestern, and some isolated regions in other areas of the study area. Low groundwater potential zones make up about 30% of the research area, whereas moderate to high groundwater potential zones cover 70% of it.

The groundwater potential map (Fig. 13c) created by ANFIS-FA shows that the east, north-central, and western parts of the research region have a low groundwater potential index, with groundwater potential index values ranging from 1.10 to 1.65. The moderate groundwater potential index was established in the north-central, central, northwest, and southwestern regions of the study area. A significant percentage of the north-central, central, southwestern, and southern parts of the research area were defined by high groundwater potential index values ranging from 1.75 to 3.70. The ANFIS-FA shows that 72% of the research region contains moderate-to-high groundwater potential zones, while 28% has low groundwater potential zones. All of the models in the study area show a high

groundwater prospect (40–45%), with approximately 28–30% of the land falling into the low prospective class (Table 2).

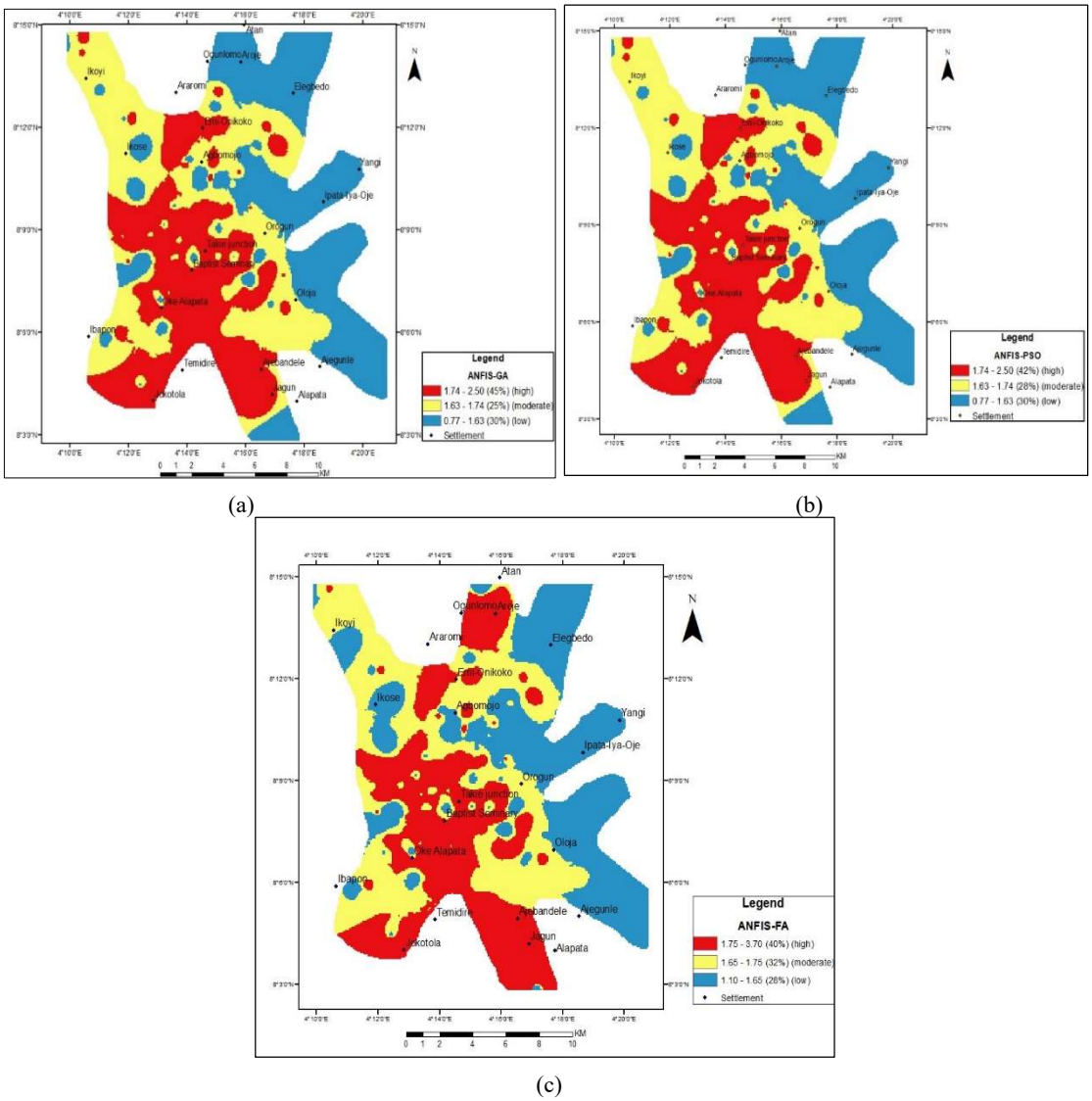

(a) (b)

(c)

Figure 13. (a) Groundwater potential map using the ANFIS–GA model (b) Groundwater potential map using the ANFIS–PSO model (c) Groundwater potential map using the ANFIS–FA model.

Table 2. Evaluation of the prospects for groundwater in Ogbomosho using a statistical comparison of ANFIS hybrid models, ANFIS-GA, ANFIS-PSO, and ANFIS-FA results.

ANFIS-GA	**Class**	**%**
1.74-2.50	High	45
1.63-1.74	moderate	25
0.77-1.63	low	30
ANFIS-PSO	**Class**	**%**
1.74-2.50	High	42
1.63-1.74	moderate	28
0.77-1.63	low	30
ANFIS-FA	**Class**	**%**
1.75-3.70	High	40
1.65-1.75	moderate	32
1.10-1.65	low	28

4-4 Validation model

4-4-1 Water column thicknesses

In order to map prospective groundwater resources using machine learning models, accurate well database information must be obtained (Nguyen et al., 2020). According to Rahmati et al. (2019) and Ozegin and Ilugbo (2024), the scientific validity of the good placements significantly impacts the standard of the findings of the availability of groundwater assessment. ArcGIS 10.2 software was adopted to generate a water column map (Fig. 14), which depicts the column of water that is supplied by the wells. The water column map of the research area shows that the amount of water in the wells is diverse by region. Low water columns (0.1–1.6) can be found in the east, northeast, and a tiny area of the northwest. The north, center, northwest, northeast, and a tiny area of the southwest have a moderate water column (1.6–2.3), according to the water column map. High-water columns (2.3–3.7) are present in the west and southwestern regions of the map. In the research area, the water column in the wells typically ranges from 0.10 to 3.70 m. The depths of the wells in the research region range from 2.4 m to 14.6 m for some, while they are shallow for others. As a result, it suggests that certain wells are replenished via surface infiltration, while others rely on the fractured basement. To validate the models, the groundwater predictive models were tied to the water columns from wells in this study location.

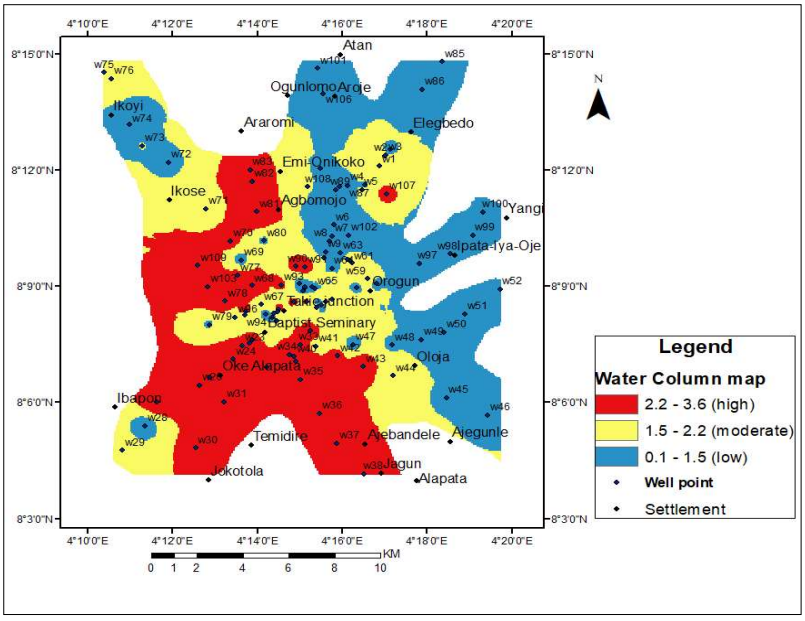

Figure 14. Water column thickness map with well distribution in the study area.

4-4-2 Groundwater potential indices

To verify the accuracy of the expected maps, data from 110 wells spanning the research region on the thickness of the water column in aquifer units was employed. The created predictive model maps were compared with the thickness of the water column map derived from the hand-dug well inventory inside the research region and superimposed on the predictive model maps to validate the groundwater predictive models. Using the linear correlation technique, the groundwater potential index of the model was contrasted with the measurements of water column thickness in wells. As shown in Fig. 15a, the ANFIS-GA groundwater potential index exhibits a

high level of collaboration with the water column thickness as demonstrated in Fig. 14. In Fig. 15b, the ANFIS-PSO groundwater potential index has a high level of correlation r = 0.77 (77%) with the water column thickness map (Fig. 14). Also, as illustrated in Fig. 15c, the ANFIS-FA groundwater potential index shows a 77% correlation with the water column thickness map. The ANFIS-GA optimizing approach offers the strongest prediction performance (80%) based on the validation of the predictive models. The three predicted models indicated that the groundwater potential in the study region is higher in the western and southwestern parts. The central, northeast, northwest, southeast, and southwest parts of the research region have moderate groundwater potential zones, while the western, northern, and a minor portion of the northwest and southwest parts have low groundwater potential zones.

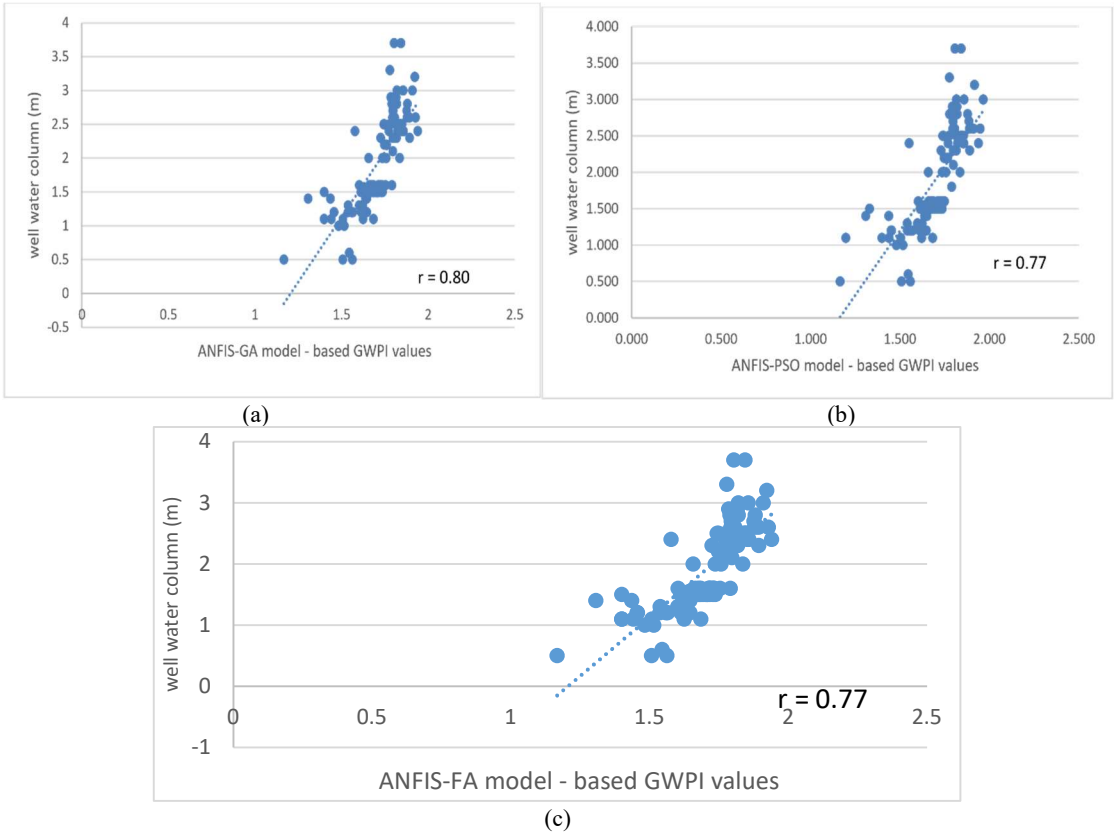

Figure 15. (a) Linear correlation of ANFIS-GA model with water column thickness in well (b) Linear correlation of ANFIS-PSO model with water column thickness in well (c) Linear correlation of ANFIS-FA model with water column thickness in well.

5 Conclusion

Remote sensing, aeromagnetic, and geophysical (involving electrical resistivity) approaches were used to gain insight into the groundwater regime of Ogbomoso, Southwestern Nigeria, to provide a solution to the issue associated with the heterogeneity phenomena in groundwater exploration of complex basement terrain. This was achieved by creating an appropriate machine learning model for projecting the best zones of groundwater resources—the optimal exploitation-optimization models. The geoelectric parameters obtained from the interpreted depth were used to obtain the second-order Dar-Zarrouk parameters, which are known as the groundwater

influencing parameters. Consideration was given to eight hydrogeological criteria (groundwater conditioning factors) that are advantageous for groundwater abstraction. The lineament density map generated for the study area shows that the southwestern part of the investigation area is characterized by a small area with high density values of 131.49–52.96 km/km². This shows a good correlation with the GA predictive model, which has a high groundwater potential index value of 1.74–2.50 in the southwestern part of the investigation area. All the groundwater predictive factors were used as input in the adaptive neuro-fuzzy inference system. The study finds that low groundwater zones make up 28% of the entire study region, while 72% of it has moderate to high groundwater potential. Using well-gathered data in the research region, the generated prospective groundwater maps were verified. The water column map in the research area and the predicted models are highly correlated. The study shows that non-linear data can be modeled using the ANFIS model, which has been improved by novel metaheuristic algorithms (ANFIS-GA, ANFIS-PSO, and ANFIS-FA). These three metaheuristic algorithms have good predictive capability, but the study also found that, with an accuracy rate of 80%, the ANFIS-GA has a greater predictive capacity than the ANFIS-PSO and ANFIS-FA. As a consequence, this study promotes the use of the adaptive techniques it implemented to train the ANFIS framework for groundwater management challenges.

References

Adeniji, A. E., Ajala, A., and Osho, J. K., 2017, Estimation of groundwater potential using surficial resistivity measurements: A case study from parts of Markurdi Benue State Nigeria: Global Journal of Pure and Applied Sciences, **23**, 311-320.

Adiat, K. A. N., Adelusi, A. O., and Ayuk, M. A., 2009, Relevance of geophysics in road failures investigation in a typical basement complex of Southwestern Nigeria: Pacific Journal of Science and Technology, **5**(2), 528-539.

Affandi, A. K., and Watanabe, K., 2007, Daily groundwater level fluctuation forecasting using soft computing technique: Nature and Science, **5**(2), 1-10.

Akinlalu, A. A., Adegbuyiro, A., Adiat, K. A. N., Akeredolu, B. E., and Lateef, W. Y., 2018, Application of multi-criteria decision analysis in prediction of groundwater resources potential: Journal of Astronomy and Geophysics, **6**(1), 184-200.

Akinluyi, A. O., Olorunfemi, M. O., and Bayowa, O. G., 2021, Application of remote sensing, GIS and geophysical techniques for groundwater potential development in the crystalline basement complex of Ondo state Southwestern Nigeria: Sustain Water Research Management, **7**(4), 1–15, https://doi.org/10.1007/s40899-020-00486-5.

AlAyyash, S., Al-Fugara, A., Shatnawi, R., Al-Shabeeb, A. R., Al-Adamat, R., and Al-Amoush, H., 2023, Combination of metaheuristic optimization algorithms and machine learning methods for groundwater potential mapping: Sustainability, **15**, 2499, https://doi.org/10.3390/su15032499.

Alipour, Z., Ali, A. M. A., Radmanesh, F., and Joorabyan, M., 2014, Comparison of three methods of ANN, ANFIS and time series models to predict ground water level: (Case study: North Mahyar Plain): Bulletin of Environment, Pharmacology and Life Sciences, **3**, 128-134.

Amutha, R., and Porchelvan, P., 2011, Seasonal prediction of groundwater levels using ANFIS and radial basis neural network: International Journal of Geology, Earth and Environmental Sciences, ISSN: 2277-2081, **1**(1), 98-108.

Ayalew, L., and Yamagishi, H., 2005, The application of GIS-based logistic regression for landslide susceptibility mapping in the Kakuda-Yahiko Mountains, Central Japan: Geomorphology, **65**, 15–31.

Azad, A., Manoochehri, M., Kashi, H., Farzin, S., Karami, H., Nourani, V., and Shiri, J., 2019, Comparative evaluation of intelligent algorithms to improve adaptive neuro-fuzzy inference system performance in precipitation modeling: Journal of Hydrology, **57**1, 214–224.

Bawallah, M. A., Aina, A. O., Ozegin, K. O., et al., 2019, Integrated geophysical investigation of aquifer and its groundwater potential in Camic Garden Estate, Ilorin Metropolis north-central basement complex of Nigeria: Journal of Applied Geology and Geophysics (IOSR-JAGG), **7**(2), 1-8, DOI: 10.9790/0990-0702010108.

Bayode, S., 2018, A geoelectric investigation of the groundwater potential in a basement complex terrain of Southwestern Nigeria: Journal of Earth and Atmospheric Research, **1**(1), 44-52.

Bayode, S., Omosuyi, G. O., Mogaji, K. A., and Adebayo, S. T., 2011, Geoelectric delineation of structurally controlled leachate plume around Otutubiosun Dumpsite, Akure, Southwestern Nigeria: Journal of Emerging Trends in Engineering and Applied Sciences (JETEAS), **2**(6), 987-994.

Bisht, D. C. S., Raju, M. M., and Joshi, M. C., 2009, Simulation of water table elevation fluctuation using fuzzy-logic and ANFIS: Computer Modeling and New Technologies, **13**(2), 16–23.

Bui, D. T., Pradhan, B., Nampak, H., Bui, Q. T., Tran, Q. A., and Nguyen, Q. P., 2016, Hybrid artificial intelligence approach based on neural fuzzy inference model and metaheuristic optimization for flood susceptibility modeling in a high-frequency tropical cyclone area using GIS: Journal of Hydrology, **540**(2), 317–330.

Chang, F. J., and Chang, Y. T., 2006, Adaptive neuro-fuzzy inference system for prediction of water level in reservoir: Advances in Water Resources, **29**, 1–10.

Chen, W., Li, H., Hou, E., Wang, S., Wang, G., and Peng, T., 2018, GIS-based groundwater potential analysis using novel ensemble weights-of evidence with logistic regression and functional tree models: Science of the Total Environment, **634**, 853–867.

Chen, W., Panahi, M., Khosravi, K., Pourghasemi, H. R., Rezaie, F., and Parvinnezhad, D., 2019, Spatial prediction of groundwater potentiality using ANFIS ensembled with teaching-learning-based and biogeography-based optimization: Journal of Hydrology, **572**, 435–448.

Chen, W., Panahi, M., and Pourghasemi, H. R., 2017, Performance evaluation of GIS-based new ensemble data mining techniques of adaptive neuro-fuzzy inference system (ANFIS) with genetic algorithm (GA), differential evolution (DE), and particle swarm optimization (PSO) for landslide spatial modeling: Catena, **157**, 310-324.

Chen, W., Panahi, M., and Pourghasemi, H. R., 2017, Performance evaluation of GIS-based new ensemble data mining techniques of adaptive neuro-fuzzy inference system (ANFIS) with genetic algorithm (GA), differential evolution (DE), and particle swarm optimization (PSO) for landslide

spatial modeling: Catena, **157**, 310-324.

Corsini, A., Cervi, F., and Ronchetti, F., 2009, Weight of evidence and artificial neural networks for potential groundwater spring mapping: an application to the Mt. Modino area (Northern Apennines, Italy): Geomorphology, **111**(1-2), 79-87.

Dan-Hassan, M. A., and Olorunfemi, M. O., 1999, Hydro-geophysical investigation of a basement terrain in the north-central part of Kaduna State: Journal of Mining and Geology, **35**(2), 189-206.

Das, S., and Pardeshi, S. D., 2018, Integration of different influencing factors in GIS to delineate groundwater potential areas using IF and FR techniques: A study of Pravara basin, Maharashtra, India: Applied Water Science, **8**, 197.

Deepesh, M., Madan, K., and Bimal, C., 2010, Assessment of groundwater potential in a semiarid region of India using remote sensing, GIS and MCDM techniques: Water Resources Management, **25**(1), 1359-1386.

Dehnavi, A., Aghdam, I. N., Pradhan, B., and Varzandeh, M. H. M., 2015, A new hybrid model using step-wise weight assessment ratio analysis (SWARA) technique and adaptive neuro-fuzzy inference system (ANFIS) for regional landslide hazard assessment in Iran: Catena, **135**, 122-148.

Edet ,A. E., Okereke, C. S., and Esu, E. O., 1998, Application of remote sensing data to groundwater exploration: a case study of the Cross River State, Southeastern Nigeria: Journal of Hydrogeology, **6**(2), 394-404.

Elmahdy, S. I., and Mohamed, M. M., 2014, Probabilistic frequency ratio model for groundwater potential mapping in Al Jaww plain, UAE: Arabian Journal of Geosciences, **8**, 2405–2416.

Elvis, B. W. W., Arsène, M., Théophile, N. M., Bruno, K. M. E., and Olivier, O. A., 2022, Integration of Shannon entropy (SE), frequency ratio (FR) and analytical hierarchy process (AHP) in GIS for suitable groundwater potential zones targeting in the Yoyo river basin, Méiganga area, Adamawa Cameroon: Journal of Hydrology: Regional Studies, **39**, 100997.

Emamgholizadeh, S., Moslemi, K., and Karami, G., 2014, Prediction of the groundwater level of Bastam Plain (Iran) by artificial neural network (ANN) and adaptive neuro-fuzzy inference system (ANFIS): Water Resources Management, **28**, 5433–5446.

Fashae, O. A., Tijani, M. N., Talabi, A. O., and Adediji, O. L., 2014, Delineation of groundwater potential zones in the crystalline basement terrain of SW-Nigeria: an integrated GIS and remote sensing approach: Applied Water Science, **4**, 19-38.

Fatoba, J. O., Omolayo, S. D., and Adigun, E. O., 2014, Using geoelectric soundings for estimation, of hydraulic characteristics of aquifers in the coastal area of Lagos: Southwestern Nigeria: International Letters of Natural Sciences, **17**(4), 338-345.

Gopinathan, P., Nandini, C. V., Parthiban, S., Sathish, S., Singh, A. K., and Singh, P. K., 2020, A geo-spatial approach to perceive the groundwater regime of hard rock terrain - a case study from Morappur area, Dharmapuri district, South India: Groundwater for Sustainable Development, https://doi.org/10.1016/j.gsd.2019.100316.

Heidari, A. A., Mirjalili, S., Faris, H., Aljarah, I., Mafarja, M., and Chen, H., 2019, Harris Hawks optimization: Algorithm and applications: Future

Generation Computer Systems, **97**, 849–872.

Hong, H., Panahi, M., Shirzadi, A., Ma, T., Liu, J., Zhu, A. X., Chen, W., Kougias, I., and Kazakis, N., 2018, Flood susceptibility assessment in Hengfeng area coupling adaptive neuro-fuzzy inference system with genetic algorithm and differential evolution: Science of the Total Environment, **621**, 1124-1141.

Honore, C. T. J., Kouadio, A. C. K., Didi, S. R. M., Diedhiou, A., and Savane, I., 2013, Groundwater exploration using extraction of lineaments from SRTM DEM and water flows in Bere region: Egyptian Journal of Remote Sensing, **24**(3), 391-400.

Huajie, D., Zhengdong, D., Feifan, D., and Daqing, W., 2016, Assessment of groundwater potential based on multicriteria decision making model and decision tree algorithms: Journal of Mathematical Problem in Engineering, **3**, 23-56.

Hussein, A. A., Govindu, V., and Nigusse, A. G. M., 2017, Evaluation of groundwater potential using geospatial techniques: Applied Water Science, **7**, 244–246.

Idiahi, E., Adiat, K. A. N., Ozegin, K. O., Salufu, S. O., Adebayo, S., and Akinlalu, A. A., 2023, The assessment of groundwater availability in sedimentary environments using the electrical resistivity method: a case of Ekpoma and its environs, Southern Nigeria: Indonesian Journal of Earth Sciences, 3(2), https://doi.org/10.52562/injoes.2023.784.

Ilugbo, S. O., Aigbedion, I., Ozegin, K. O., and Bawallah, M. A., 2023a, Assessment of groundwater occurrence in a typical schist belt region in Osun State, Southwestern Nigeria using VES, aeromagnetic dataset, remotely sensed data, and MCDA approaches: Sustainable Water Resources Management, **9**, 29, https://doi.org/10.1007/s40899-022-00810-1.

Ilugbo, S. O., Aigbedion, I., and Ozegin, K. O., 2023b, Structural mapping for groundwater occurrence using remote sensing and geophysical data in Ilesha Schist Belt, Southwestern Nigeria: Geology, Ecology, and Landscapes, 1-18, https://doi.org/10.1080/24749508.2023.2182063.

Jaafari, A., Termeh, S. V. R., and Bui, D.T., 2019, Genetic and firefly metaheuristic algorithms for an optimized neuro-fuzzy prediction modeling of wildfire probability: Journal of Environmental Management, **243**, 358-369.

Jang, J. S., 1993, Adaptive-network-based fuzzy inference system: IEEE Transactions on Systems, Man, and Cybernetics, **23**, 665–685.

Jhan, M., Chowdary, V., and Chowdhury, A., 2012, Groundwater assessment in Salboni Block, West Bengal, India using remote sensing, geographic information system and multi-criteria decision analysis techniques: Hydrogeology Journal, **18**, 1713–1728.

Julla, K., Dereje, A., Motuma, S. R., and Megersa, K. L., 2022, Groundwater potential assessment using GIS and remote sensing techniques: case study of West Arsi Zone, Ethiopia: Water, **14**(12), 1838.

Karamouz, M., Tabari, M. M. R., and Kerachian, R., 2007, Application of genetic algorithms and artificial neural networks in conjunctive use of surface and groundwater resources: Water International, **32**(1), 163–176.

Keary, P., and Brooks, M., 2002, An Introduction to Geophysical Exploration, third edition: Blackwell Publishing, 155-198.

Keller, G. V., and Frischknecht, F. C., 1966, Electrical Methods in

Geophysical Prospecting: Pergamon Press Inc., Oxford, 2nd edition, 33-40.

Kennedy, J., and Eberhart, R., 1995, Particle Swarm Optimization: Proceedings of ICNN'95 International Conference on Neural Networks, Perth, WA, Australia, 27 November–December 1995, IEEE, https://doi.org/10.1109/ICNN.1995.488968.

Khabat, K., Mahdi, P., and Dieu, T. B., 2018, Spatial prediction of groundwater spring potential mapping based on an adaptive neuro-fuzzy inference system and metaheuristic optimization: Journal of Hydrology and Earth System Sciences, **22**(9), 4771–4792.

Khosravi, K., Nohani, E., Maroufinia, E., and Pourghasemi, H. R., 2016, A GIS-based flood susceptibility assessment and its mapping in Iran: a comparison between frequency ratio and weights-of-evidence bivariate statistical models with multi-criteria decision-making technique: Natural Hazards, **83**, 947–987.

Khosravi, K., Panahi, M., and Tien Bui, D., 2018, Spatial prediction of groundwater spring potential mapping based on an adaptive neuro-fuzzy inference system and metaheuristic optimization: Hydrology and Earth System Sciences, **22**, 4771–4792, https://doi.org/10.5194/hess-22-4771-2018.

Kumar, P., Herath, S., Avtar, R., and Takeuchi, K., 2016, Mapping of groundwater potential zones in Killinochi area, Sri Lanka, using GIS and remote sensing techniques: Sustainable Water Resources Managment, **2**, 419–430.

Lee, S., Hong, S. M., and Jung, H. S., 2018, GIS-based groundwater potential mapping using artificial neural network and support vector machine models: the case of Boryeong city in Korea: Geocarto International, **33**(8), 847-861.

Lee, S., Song, K. Y., Kim, Y., and Park, I., 2012, Regional groundwater productivity potential mapping using a geographic information system (GIS) based artificial neural network model: Hydrogeology Journal, **20**(8), 1511-1527.

Mah, A., Taylor, G. R., Lennox, P., and Balia, L., 1995, Lineament analysis of landsat thematic mapper images, Northern Territory, Australia: Photogrammetric Engineering & Remote Sensing, **61**(6), 761–773.

Maiti, S., and Tiwari, R. K., 2014, A comparative study of artificial neural networks, Bayesian neural networks and adaptive neuro-fuzzy inference system in groundwater level prediction: Environmental Earth Sciences, **71**, 3147–3160.

Maity, B., Mallick, S. K., Das, P., and Rudra1, S., 2022, Comparative analysis of groundwater potentiality zone using fuzzy AHP, frequency ratio and Bayesian weights of evidence methods: Applied Water Science, **12**, 63.

Maniar, H. H., Bhatt, N. J., Prakash, I., and Mahmood, K., 2017, Application of analytical hierarchy process (AHP) and GIS in the evaluation of groundwater recharge potential of Rajkot District, Gujarat, India: International Journal of Technical Innovation in Modern Engineering and Science, **5**, 1078–1087.

Mayilvaganan, M. K., and Naidu, K. B., 2012, Application of soft computing techniques for groundwater level forecasting: International Conference on Computer Networks and Communication Systems (CNCS 2012) IPCSIT 5, IACSIT Press, Singapore, 2012.

Milan, S. G., Roozbahani, A., and Banihabib, M. E., 2018, Fuzzy optimization model and fuzzy

inference system for conjunctive use of surface and groundwater resources: Journal of Hydrology, **566**, 421–434.

Mogaji, K. A., Olayanju, G. M., and Oladapo, M. I., 2011, Geophysical evaluation of rock type impact on aquifer characterization in basement complex areas of Ondo State, Southwestern Nigeria: Geoelectric and geographical information system approach: International Journal of Water Resources and Environmental Engineering, **3**(4), 77-86.

Mrinal, R., 2009, Nevanlinna–Pick interpolation for C+BH∞, Integral Equations Operator Theory: SP Birkhäuser Verlag Basel, **63** (1), 103–125.

NGSA, 2010, Nigeria Geological Survey Agency: The Geological Survey of Nigeria, 1:100000 Sheet 223.

Nguyen, P. T., Ha, D. H., Jaafari, A., et al., 2020, Groundwater potential mapping combining artificial neural network and real AdaBoost ensemble technique: the Daknong province case-study, Vietnam: International Journal of Environmental Research and Public Health, **17**(7), 2473, https://doi.org/10.3390/ijerph17072473.

National Population Commission (NPC), 2006, Nigeria National Census: Population Distribution by Sex, State, LGAs and Senatorial District: 2006 Census Priority Tables (Vol. 3), http://www.population.gov.ng/index.php/publication/140-popn-distri-by-sex-state-jgas-and-senatorial-distr-2006.

Okhue, I. T., and Olorunfemi, M. O., 1991, Electrical resistivity of a typical basement complex area: The Obafemi Awolowo university campus case study: Journal of Mining and Geology, **27**(2), 66-70.

Olorunfemi, M. O., and Oloruniwo, M. A., 1985, Parameters and aquifer characteristics of some parts of Southwestern Nigeria: Geologia Applicata Idrogeologia, **20**(1), 99-109.

Omosuyi, G. O., Ojo, J. S., and Enikanselu, P. A., 2003, Geophysical investigation for groundwater around Obanla-Obakekere in Akure Area within the basement complex of Southwestern Nigeria: Journal of Mining and Geology, **39**(2), 109-116.

Ozdemir, A., 2011, GIS-based groundwater spring potential mapping in the Sultan Mountains (Konya, Turkey) using frequency ratio, weights of evidence and logistic regression methods and their comparison: Journal of Hydrology, **411**, 290–308.

Ozegin, K. O., and Alile, O. M., 2021, Depth estimation based on Fourier spectral analysis of potential field data: The Nigerian Research Journal of Engineering and Environmental Sciences, **6**(2), 540–547, http://doi.org/10.5281/zenodo.5805122.

Ozegin, K. O., and Alile, O. M., 2023, Structural deformation analysis of parts of Nigeria's Southwestern Precambrian basement complex using gradient techniques: Iranian Journal of Geophysics, **16** (4), 193–209, https://doi.org/10.30499/IJG.2023.350802.1442.

Ozegin, K. O., Ilugbo, S. O., and Adebo, B., 2024, Spatial evaluation of groundwater vulnerability using the DRASTIC-L model with the analytic hierarchy process (AHP) and GIS approaches in Edo State, Nigeria: Physics and Chemistry of the Earth, **134**, 103562, https://doi.org/10.1016/j.pce.2024.103562.

Ozegin, K. O., Ilugbo, S. O., and Ogunseye, T. T., 2023, Groundwater exploration in a landscape with heterogeneous geology: An application of geospatial and analytical hierarchical process (AHP) techniques in the Edo north region, in

Nigeria: Groundwater for Sustainable Development, **20**(2), 100871, https://doi.org/10.1016/j.gsd.2022.100871.

Ozegin, K. O., and Ilugbo, S. O., 2024, A triangulation approach for groundwater potential evaluation using geospatial technology and multi-criteria decision analysis (MCDA) in Edo State, Nigeria: Journal of African Earth Sciences, **209**, 105101, https://doi.org/10.1016/j.jafrearsci.2023.105101.

Ozegin, K. O., Isiwele, D. O., and Azi, S. O., 2007, Groundwater potential investigation using combined VLF and VES: Journal of the Nigeria Association of Mathematical Physics, **11**, 403-410, DOI:10.4314/jonamp.v11i1.40235.

Parasnis, D. S., 1986, Principles of Applied Geophysics, 3rd edition: Champman & Hall, New York, 33-42.

Rahaman, M. A., 1976, Review of the basement geology of Southwestern Nigeria, in Kogbe, C. A., ed., Geology of Nigeria, 2nd edition: Elizabethan Publishers, Lagos, Nigeria, 41–58.

Rahaman, M. A., 1988, Recent advances in the study of the basement complex of Nigeria, in Oluyide, P. O., Mbonu, W. C., Ogezi, A. E. E., Egbuniwe, I. G., Ajibade, A. C., Umeji, A. C., eds., Precambrian Geology of Nigeria: G.S.N., 11-41.

Rahmati, O., Moghaddam, D. D., Moosavi, V., Kalantari, Z., Samadi, M., Lee, S., and Tien Bui, D., 2019, An automated Python language-based tool for creating absence samples in groundwater potential mapping: Remote Sensing, **11**(11), 1375, https://doi.org/10.3390/rs11111375.

Rezaei, F., Safavi, H. R., and Zekri, M., 2017, A hybrid fuzzy-based multi-objective PSO algorithm for conjunctive water use and optimal multi-crop pattern planning: Water Resources Management, **31**(4), 1139–1155.

Roy, D. K., Barzegar, R., Quilty, J., and Adamowski, J., 2020, Using ensembles of adaptive neuro-fuzzy inference systems and optimization algorithms to predict reference evapotranspiration in subtropical climatic zones: Journal of Hydrology, **591**, 125509, https://doi.org/10.1016/j.jhydrol.2020.125509.

Sahoo, S., Jha, M. K., Kumar, N., and Chowdary, V. M., 2015, Evaluation of GIS-based multicriteria decision analysis and probabilistic modeling for exploring groundwater prospects: Environmental Earth Sciences, **74**, 2223–2246.

Shenyong, R., and Ruiqiu, H., 2001, Application of GIS-based information model on assessment of geological hazards risk: Journal of Chengdu University of Technology, **28**(1), 89-92.

Singh, A. K., and Prakash, S. R., 2002, An integrated approach of remote sensing, geophysics and GIS to the evaluation of groundwater potentiality of Ojhala sub-watershed, Mirjapur district, UP, India: Asian conference on GIS, GPS, aerial photography and remote sensing, Bangkok, Thailand, 7–9 August 2002.

Sokeng, V. J., Kouamé, F., Ngatcha, B. N., N'da, H. D., You, L. A., and Rirabe, D., 2016, Delineating groundwater potential zones in Western Cameroon Highlands using GIS based artificial neural networks model and remote sensing data: International Journal of Innovation and Applied Studies, **15**(4), 747-759.

Tahmassebipoor, N., Rahmati, O., Noormohamadi, F., and Lee, S., 2016, Spatial analysis of groundwater potential using weights-of-evidence and evidential belief function models

and remote sensing: Arabian Journal of Geosciences, **9**(1), 1-18.

Takagi, T., and Sugeno, M., 1985, Fuzzy identification of systems and its applications to modeling and control: IEEE Transactions on Systems, Man, and Cybernetics, **SMC-15**, 116–132.

Tehrany, M. S., Pradhan, B., and Jebur, M. N., 2013, Spatial prediction of flood susceptible areas using rule based decision tree (DT) and a novel ensemble bivariate and multivariate statistical models in GIS: Journal of Hydrology, **504**, 69–79.

Termeh, S. V. R., Khosravi, K., Sartaj, M., Keesstra, S. D., Tsai, F. T. C., Dijksma, R., and Pham, B. T., 2019, Optimization of an adaptive neuro-fuzzy inference system for groundwater potential mapping: Hydrogeology Journal, **27**(7), 2511-2534.

Tesfaye, T., 2014, Ground water potential evaluation based on integrated GIS and remote sensing techniques, in Bilate River Catchment: South Rift Valley of Ethiopia: American Academic Scientific Research Journal for Engineering Technology and Sciences, **10**, 85–120.

Todd, D. K., and Mays, L.W., 1980, Groundwater Hydrology, 2nd edition: Wiley, New York.

Tsakiri, K., Marsellos, A., and Kapetanakis, S., 2018, Artificial neural network and multiple linear regression for flood prediction in Mohawk River, New York: Water, **10**(9), 1158.

Umar, Z., Pradhan, B., Ahmad, A., Jebur, M. N., and Tehrany, M. S., 2014, Earthquake induced landslide susceptibility mapping using an integrated ensemble frequency ratio and logistic regression models in West Sumatera Province, Indonesia: Catena, **118**, 124–135.

Vander Velpen, B. P. A. (2004). WinRESIST Version 1.0 Resistivity Depth Sounding Interpretation Software. Delf, the Netherland: ITC.

Wen, X., Feng, Q., Yu, H., Wu, J., Si, J., Chang, Z., and Xi, H., 2015, Wavelet and adaptive neuro-fuzzy inference system conjunction model for groundwater level predicting in a coastal aquifer: Neural Computing and Applications, **26**, 1203–1215.

Xu, C., Xu, X., Dai, F., Xiao, J., Tan, X., and Yuan, R., 2012, Landslide hazard mapping using GIS and weight of evidence model in Qingshui River watershed of 2008 Wenchuan earthquake struck region: Journal of Earth Science, **23**, 97–120.

Yang, X. S., 2009, Firefly algorithms for multimodal optimization, in Watanabe, O., Zeugmann, T., eds., Stochastic Algorithms: Foundations and Applications, SAGA 2009, Lecture Notes in Computer Science, **5792**: Springer, Berlin, Heidelberg, https://doi.org/10.1007/978-3-642-04944-6_14.

Zandi, J., Ghazvinei, P. T., Hashim, R., Yusof, K. B. W., Ariffin, J., and Motamedi, S., 2016, Mapping of regional potential groundwater springs using logistic regression statistical method: Water Resources **43**, 48–57.